

Structural Optimization of Regeneratively Cooled Rotating Detonation Rocket Engines

by

Eric D. Jorgensen

B.S. Mechanical Engineering
Worcester Polytechnic Institute, 2016

Submitted to the Department of Mechanical Engineering
in partial fulfillment of the requirements for the degree of

Master of Science in Mechanical Engineering

at the

MASSACHUSETTS INSTITUTE OF TECHNOLOGY

February 2022

© Massachusetts Institute of Technology 2022. All rights reserved.

Signature of Author: _____
Department of Mechanical Engineering
January 7, 2022

Certified by: _____
Zachary Cordero
Assistant Professor
Thesis Supervisor

Certified by: _____
Ahmed Ghoniem
Professor
Department Reader

Accepted by: _____
Nicolas Hadjiconstantinou
Chairman, Department Committee on Graduate Theses

Structural Optimization of Regeneratively Cooled Rotating Detonation Rocket Engines

by

Eric D. Jorgensen

Submitted to the Department of Mechanical Engineering
in February 2022, in partial fulfillment of the
requirements for the degree of
Master of Science in Mechanical Engineering

Abstract

Combustors in rotating detonation rocket engines (RDREs) must withstand prolonged exposure to high heat fluxes ($>10 \text{ MW/m}^2$) and ultrasonic-frequency detonative loading. Regenerative cooling is being considered for thermal management in RDREs, but there is concern that the cooling channels may fail by fatigue due to the detonative loads. In the present work a structural optimization protocol for regeneratively cooled RDREs is developed and then used to determine optimal cooling channel geometries which minimize thermomechanical stresses that might drive such failures. The analysis considers thermal stresses from temperature gradients through the combustor wall, bending stresses due to cooling channel pressurization, and dynamic stresses from detonative loading. To calculate the dynamic stresses, the combustor hot wall is approximated as a beam on an elastic foundation, where the stiffness of the elastic foundation is a function of the cooling channel geometry and the properties of the combustor material. The structural optimization framework is applied to an exemplary RP2/GOX RDRE combustor, and optimal designs are determined as a function of propellant flow rate for several candidate combustor materials – GRCo-84, IN718, W-25Re, Nb-C103. The deviatoric stress in the hot wall increases monotonically with propellant flow rate. In all cases onset of yielding limits the maximum achievable flow rate. W-25Re can achieve the highest propellant flow rate of the materials considered here, owing to its combination of high thermal conductivity and high strength at elevated temperatures. While thermal stresses dominate most of the design space for each material, dynamic stresses become significant when the detonation wave speed approaches the elastic wave speed of the hot wall. This effect is important in Nb-C103, GRCo-84, and W-25Re combustors, since the detonation wave speed matches the elastic wave speed for cooling channel designs that minimize static stresses. These results highlight the importance of dynamic stresses in regeneratively cooled RDREs, as combustor designs which minimize static stresses can sometimes amplify dynamic stresses, mitigating creep but promoting fatigue.

Thesis Supervisor: Zachary Cordero
Title: Assistant Professor
Thesis Reader: Ahmed Ghoniem
Title: Professor

Acknowledgements

The submission of this thesis is the final step in an MIT journey that began nearly 3.5 years ago, with the research of this thesis itself beginning about 1.5 years ago. This adventure has been a major commitment and I would not be where I am today without the unwavering support, throughout it all, from a large network of people. Thank you to all the professors, fellow students, co-workers, friends, and family that played a part in making this experience and accomplishment both rewarding and possible.

Emily, at the very beginning of my first class at MIT, you worried that my commitment to school would prevent me from being able to carve out enough time to foster a serious relationship. Fast forward over 3 years and here we are, married, yet still working on finishing up at MIT. You have been with me throughout this entire journey for all the highs and all the lows. This accomplishment is just as much as yours as it is mine. Thanks for keeping me sane through sleepless nights and keeping me fed through times where I felt I could not spare a minute. The thought of freeing up additional time to spend with you has been my greatest motivator to finishing school.

Dad, Mom, Grant, and Danica, thank you for encouraging me to give this a shot in the first place. Thank you for your continuous prayers and support from day one. You were always patient and understanding of my commitments to school and worked our family's schedule around those obligations. Thank you for picking me up when I was down and celebrating each of the many milestones along the way.

Zack, thank you for bringing me into your lab and for your huge commitment in mentorship and guidance throughout this research effort. You seemed to always be able to steer me back on track when I felt lost and you would roll up your sleeves to dive into the details when I was truly stuck. It has been a privilege to learn from you, particularly your work ethic and attention to detail, and I look forward to applying my learnings throughout my engineering career.

Dr. Jeff Wegener, thank you for sharing your expertise on rotating detonation rocket engines to ensure that our research effort would be a meaningful contribution to further their development.

Prof. Natasha Vermaak, thank you for your time spent reviewing our work and your guidance in how to visualize optimization results in a meaningful and intuitive way.

To my friends, thank you all for your support throughout my time at MIT. You all were there to provide much needed distractions to help me recharge when my battery was running low.

To my managers, mentors, and peers at GE, thank you for your encouragement and support to pursue this path at MIT. I would not have even attempted this path without your belief in me. Thank you GE for sponsoring my tuition and investing in me to make this opportunity a possibility in the first place.

To my dear friend Jeremy, losing such a close friend such as yourself was an utter tragedy. It put me in quite the tailspin as I tried to maintain some level of focus to finish writing and refining

this paper, but I know that getting over the finish line is what you would have wanted for me. I wish that you were still here to celebrate this milestone in my life, but I am so grateful to have been your friend and known you as long as I have. You truly were one of a kind and the world needs more people like you.

Thank you God for the opportunity to pursue a degree at MIT and for giving me all the gifts necessary to make this a reality. This journey was a testament to Philippians 4:13 "I can do all this through him who gives me strength."

Contents

Abstract	3
Acknowledgements	5
Chapter 1: Introduction	15
1.1. Background	17
1.2. Motivation	20
1.3. Outline	21
Chapter 2: Combustor design assumptions and boundary condition setup	22
2.1. Combustor geometry	22
2.2. Combustor materials	23
2.3. Combustion behavior	24
2.4. Fuel properties	25
Chapter 3: Thermomechanical modeling	26
3.1. Bending stress	26
3.2. Thermal stress	26
3.3. Detonative stress	30
3.4. Regenerative cooling considerations	32
Chapter 4: Results and discussion	33
Chapter 5: Conclusions	40
5.1. Combustor design key results	40
5.2. Future work	41
Appendix	43
Bibliography	56

List of Figures

Figure 2-1: (a) Exemplary RDRE combustor. (b) Section view of cooling channels.	23
Figure 2-2: Yield strength (σ_y) and Young's modulus (E) of candidate combustor materials.	24
Figure 3-2: Cooling channel half unit cell with labeling to indicate nodes in thermal resistor network.	29
Figure 3-3: Combustor wall as a beam on an elastic foundation.	30
Figure 4-1: (a) Design map for regeneratively cooled GRCop-84 RDRE combustors with iso-contours of constant σ_{VM}/σ_y . Fixed parameters include: $h = 0.5$ mm, $b = 1$ mm, and $\dot{m}_f = 1$ kg/s. The red contour denotes designs for which $\Delta p = 1.5$ MPa. Viable designs which satisfy the different design and performance constraints are highlighted green. The filled marker indicates the optimal design which minimizes stress σ_{VM}/σ_y . (b) von Mises, thermal, bending, and dynamic stresses plotted against hot wall thickness for the same conditions as in (a), with the additional constraint $s = 1.55$ mm.	34
Figure 4-2: Cooling channel dimensions which minimize normalized effective stress (σ_{VM}/σ_y) at a given mass flow rate while satisfying constraints on pressure drop ($\Delta p < 1.5$ MPa), fuel temperature ($T_f < 600$ K), and metal temperature ($T_{max} < T_{service}$).	35
Figure 4-3: Constraint activity parameters vs. fuel flow rate for optimal cooling channel configurations in Fig. 4-2.	37
Figure 4-4: Areal density of optimal combustor designs vs. fuel flow rate.	38
Figure 4-5: V_{CJ}/V_{Cr} versus fuel flow rate for different combustor materials. Note Nb-C103, W-25Re, GRCop-84 combustors all avoid the critical condition, $V_{Cr} = V_{CJ}$, when dynamic stresses are considered.	39

Figure 5-1: Chapman-Jouguet parameters for a pre-vaporized RP2/GOX detonation reaction as functions of equivalence ratio ϕ	42
---	----

List of Tables

Table 1-1: Most common detonation-based engine configurations with example schematics and summary details.	17
Table 1-2: Summary of relevant RDRE test runs.	18
Table 2-1: Material properties of candidate combustor materials.	24

Nomenclature

b	=	land thickness (m)
$C_{p,f}$	=	specific heat of fuel (kJ/kg-K)
D	=	combustor diameter, at the hot wall surface (m)
E	=	Young's modulus (Pa)
f	=	friction factor
f_w	=	axial line fraction of combustor occupied with solid material
h	=	cooling channel height (m)
h_f	=	convective heat transfer coefficient of the fuel (W/m ² -K)
K	=	elastic foundation stiffness (N/m ²)
L	=	axial length of the combustor (m)
m	=	beam mass per unit length (kg/m)
\dot{m}_f	=	mass flow rate of fuel (kg/s)
P_{CJ}	=	Chapman-Jouguet pressure (Pa)
p	=	cooling channel internal pressure (Pa)
q	=	heat flux into the combustor wall (W/m ²)
s	=	cooling channel width (m)
T_f	=	fuel temperature (K)
V_{CJ}	=	Chapman-Jouguet velocity (m/s)
V_{Cr}	=	critical velocity (m/s)
α	=	coefficient of thermal expansion (K ⁻¹)
Δ	=	combustor hot wall thickness (m)
Δp	=	cooling channel pressure drop (Pa)
κ	=	thermal conductivity (W/m-K)
κ_f	=	thermal conductivity, fuel (W/m-K)
λ	=	static wave characteristic length (1/m)
μ	=	dynamic viscosity (Pa-s)

ν	=	Poisson's ratio
ρ	=	density (kg/m ³)
ρ_f	=	density, fuel (kg/m ³)
σ_{VM}	=	von Mises equivalent stress (Pa)
σ_y	=	0.2% yield strength (Pa)

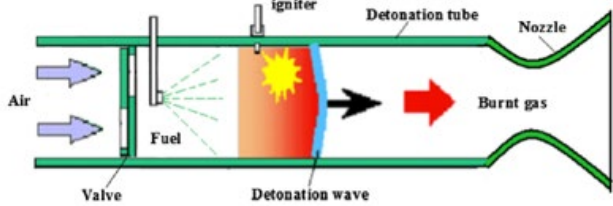
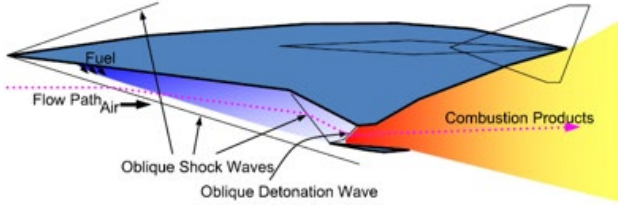
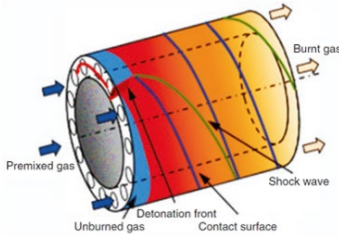
Chapter 1: Introduction

Detonation-based, pressure gain combustion (PGC) propulsion systems generate thrust by expelling exhaust gases following a supersonic detonation reaction rather than a more conventional, deflagration reaction. There is a renewed interest in detonation engines due to their opportunity for compact size [1–3] and theoretical efficiency [1,3,4] which make them attractive for size, weight, and power constrained space propulsion applications. Their compact size stems from a reduction in the required length to sustain a detonation reaction rather than a deflagration reaction [1]. For example, the detonation height of certain hydrocarbon and oxygen mixtures is on the order of centimeters while deflagration combustors with the same chemistry can have characteristic lengths on the scale of a meter [2,3]. Hargus et al. mention the overall engine architecture can be simplified since the combustion reaction results in a pressure gain, thus reducing the demand on upstream turbomachinery to increase pressure which presents another opportunity for system size reduction [4]. Additionally, Boller [1], Braun et al. [3], and Hargus et al. [4], among other researchers [5,6], have theorized that a detonation reaction can be more efficient than deflagration because the rapid reaction time prevents expansion of the reacting gases, resulting in a near isochoric reaction. The heat addition in the isochoric reaction leads to lower entropy production than the approximately isobaric deflagration reaction.

Several different detonation propulsion concepts have been pursued, including pulse detonation engines (PDEs), standing detonation engines (SDEs), and rotating detonation engines (RDEs) [6]. To clarify, an RDRE is specifically the rocket application of the broader RDE category. A PDE operates with repetitive, discrete detonation reactions by introducing propellants into the combustion chamber, initiating a detonation, and expelling the expanded byproducts to produce thrust [7]. Proposed configurations feature multiple combustion chambers in parallel to attempt obtaining quasi steady state thrust output. However, one drawback to this technique is that it is not self-sustaining, each detonation requires an initiation. Therefore, increasing the number of combustion chambers to achieve near steady state thrust becomes costly when expending energy to initiate detonations at such high frequencies. SDEs, also known as oblique detonation wave engines (ODWEs), are a type of continuous detonation engine [3]. The goal of this technology is

to sustain the detonation wave, fixed in space, inside the combustor. It requires supersonic flow inlet conditions and introduces propellants in this flow, upstream from the combustor, to drive the detonation reaction to produce thrust. The necessity for supersonic inlet conditions limits the widespread use of this technology primarily to hypersonic flight vehicles. Lastly, RDEs are another type of a continuous detonation engine [8]. In this configuration, detonation waves are sustained in the flowpath annulus by injecting fuel and oxidizer into the combustor ahead of the circumferentially traveling detonation waves. RDEs are most promising due to their capability for achieving nearly constant thrust output, compatibility with conventional input fuel and oxidizer conditions, and having a self-sustaining detonation reaction. However, the high frequency, detonative loading present in an RDE and more specifically, an RDRE, has limited the clarity of experimental assessments of efficiency (e.g., through I_{sp} measurements). These technical challenges with extended operation of RDREs are discussed later in this chapter. A summary of the different detonation engine configurations is shown in **Table 1-1**.

Table 1-1: Most common detonation-based engine configurations with example schematics and summary details.

engine	schematic	details
PDE [8]		<ul style="list-style-type: none"> • ignition needed for each detonation • typical engine inlet conditions • intermittent thrust output • broadest experience base
SDE [9]		<ul style="list-style-type: none"> • ignition only at start, self-sustaining • high speed/supersonic inlet conditions • constant thrust output • smallest experience base
RDE [10]		<ul style="list-style-type: none"> • ignition only at start, self-sustaining • typical engine inlet conditions • constant thrust output • intermediate experience base

1.1. Background

RDRE research began when Voitsekhovskii theorized that a detonation wave could follow a helical path within a tube by burning a shock-compressed mixture of fuel and oxygen ahead of the moving wave [12,13]. The mixture of fuel and oxygen would then be replenished behind the moving shock for the next time the wave passed that fixed location within the tube. In 1960, Voitsekhovskii observed the spinning detonation phenomena experimentally while using a gaseous acetylene and oxygen mixture with a center fed planar combustion chamber [4,12].

Despite RDRE research dating back to the 1960s, the longest test run for an RDRE has only been about 10 seconds [14]. These short duration test fires are due to the harsh operating conditions which subject the combustor to high heat fluxes and ultrasonic-frequency detonative loading. Time-average measurements of the heat flux in RDREs range from 4 MW/m² in a C₂H₄/GOX RDRE [14] to ~25 MW/m² in a CH₄/GOX RDRE [15]. A summary of various RDRE test runs are highlighted in **Table 1-2**.

Table 1-2: Summary of relevant RDRE test runs.

combustor material	fuel	oxidizer	ϕ	\dot{m}_f (kg/s)	run time (s)	q (MW/m ²)	reference
copper	ethylene	oxygen	< 1	0.143	< 1	8.1	[11]
copper with c/c liner	ethylene	oxygen	1.63	0.096	10.2	4	[14]
copper with c/c liner	ethylene	oxygen	0.9	0.214	6.3	7.25	[14]
copper	hydrogen	oxygen	1.17	1.16	< 1	23	[15]
copper	methane	oxygen	1.15	0.84	< 1	25	[15]

Although the table presents the time-average measurement of the heat flux, considering the general structure of the passing detonation wave reveals the local peak heat fluxes directly beneath the wave would be on the order of 100 MW/m². Theurerkauf et al. used resistance temperature detectors (RTDs) to measure the heat flux into the combustor wall in RDE test firings at a fixed location on the combustor wall [16]. At this fixed location, the detonation wave pulsed about every 0.5 milliseconds and it took approximately 0.03 milliseconds for the peak of the detonation heat flux measurement to decay back to near 0. By assuming the detonation heat flux follows that of a decaying exponential of form $q_{peak} = qe^{-t/\tau}$ and an average heat flux, q , of 5 MW/m², the peak heat flux, q_{peak} , nearly reaches 100 MW/m².

Based on the heat flux data in liquid rocket engines compiled by Pizzarelli, the local heat flux at the throat section of the nozzle is of the same order of magnitude as the peak RDRE heat flux [17]. However, the liquid rocket engine data set features combustors run at conventional rocket engine pressures. As noted by Hargus et al., to align with conventional rocket engine pressures, the operational pressure of RDREs tested to date would need to be scaled up by 10-100 times.

Although the scaling relationship between heat flux and chamber pressure in an RDRE is unknown at this time, there is concern that increasing chamber pressure will decrease the detonation cell size. A smaller detonation cell size would likely result in higher heat fluxes [4].

At the presently reported RDRE heat fluxes, 1D heat transport calculations show that such conditions will melt most combustor materials in several 100 milliseconds. For instance, assuming a mean heat flux of 5 MW/m² into the combustor wall and using,

$$t = \frac{(T_m - T_{amb})(\rho C_p k_{th})^{1/2}}{q \left(\frac{\pi}{2}\right)^{1/2}}, \quad (1 - 1)$$

the estimated time for the combustor to reach its melting point is ~500 milliseconds for C1100 and ~250 milliseconds for Al 6061 and IN718. These calculation show RDREs cannot sustain extended operation without thermal management.

To manage the extreme thermal environment, researchers have been exploring options such as flowpath coolant injection, high temperature materials, and active cooling schemes. Kasahara et al. ran their C1100 RDRE with ethylene and gaseous oxygen at equivalence ratios ranging from 0.24-1.68 as well as different nozzle configurations to a maximum test duration of two seconds [18]. These investigators explored direct injection of water into the combustor and measured changes in temperature rise and heat flux. The results demonstrated a 33% reduction in peak temperature rise measured 2 mm from the combustion flowpath. Ishihara et al. sought to sustain long duration testing by introducing a high temperature capable C/C composite material and tailoring the injector design to mitigate the heat flux intensity into the combustor wall [14,19]. They were able to achieve 6 and 10 second test firings with ethylene-oxygen propellants at equivalence ratios of 0.90 and 1.63, respectively. However, the composite liner sustained erosion from the detonations to depths ranging from 50 to 1000 micrometers. Regenerative cooling has been proposed to manage these extreme thermal loads [20], but there are concerns that the thin hot wall will fail under the combined action of thermal stresses, bending stresses from cooling channel pressurization, and dynamic stresses from detonative loading.

1.2. Motivation

To better understand the capabilities of the RDRE technology in experimentation and to enable their use in future spacecraft applications, we must achieve operation times that extend beyond the current state-of-the-art. One of the first steps to extending RDRE operation times is understanding the capability of an actively cooled combustor when subjected to the high heat flux, ultrasonic-frequency, detonative loading. Previous work has examined separately the thermal and bending stresses in regeneratively cooled combustors [21–24] and the structural response of enclosures to internal detonations [25,26].

Valdevit and co-workers developed a structural optimization framework for regeneratively cooled scramjet panels where detonative loads are absent [21–24]. The analysis was based on a 2-D thermal resistance network to model temperatures within a fuel cooled combustor panel with rectangular cooling channels. Stresses were then calculated based on the temperatures and pressures using beam bending relationships. Their framework determined cooling channel geometries that minimize weight while ensuring the hot wall does not yield due to thermal or bending stresses. They applied their framework to several different candidate combustor materials and demonstrated that the optimal cooling channel design varies in non-intuitive ways depending on the material properties and the operating conditions.

A key aspect of RDRE design which differs from the scramjet problem is the presence of a detonative load source. Tang studied the effects of an internal moving pressure load in cylindrical tubes [25]. He identified different deflection behaviors based on the relationship between the velocity of the moving pressure wave and the shear and dilatational wave speeds in the cylinder. These material-based characteristic wave speeds were referred to as critical wave speeds and, depending on the proximity of the load source velocity to a critical wave speed, determined the peak deflection in the tube. Tang found that the dynamic deflection could be as much as 2.5 times higher than that induced by the otherwise equivalent static loading condition.

Beltman and Shepherd later expanded these results to thin cylindrical shells subjected to internal detonative loading [26]. They experimentally confirmed a stress amplification effect, observing stresses 3–4 times higher than those expected under equivalent static loads. Such stress

amplification effects might be important in RDREs where they can drive fatigue, although to our knowledge, they have not previously been considered.

The aim of this research is to determine optimal cooling channel geometries which simultaneously minimize the static and dynamic stresses in an exemplary regeneratively cooled RP-2/GOX RDRE. To this end, the structural optimization framework developed by Valdevit and co-workers is modified to include detonative loading. The framework is then used to compute optimal cooling channel geometries for several candidate combustor materials – GRCop-84, IN718, W-25Re, Nb-C103 – over a range of propellant flow rates. The present analysis shows that cooling channel designs which minimize static stresses can sometimes amplify dynamic stresses, suppressing creep but promoting fatigue. While this paper focuses on a specific combustor design and propellant chemistry, the structural optimization framework developed here can be extended to other pressure gain combustion architectures, propellant chemistries, and combustor materials.

1.3. Outline

The thesis is organized as follows: Chapter 2 presents the setup of the problem. This consists of the relevant geometric parameters, material property assumptions, and fuel characteristics as they pertain to cooling and detonation properties. Chapter 3 is a guide through the analysis steps and equations used to determine the equivalent stress value for a given combustor design configuration. The results are obtained by combining the static thermal and mechanical stresses with the dynamic stresses. Chapter 4 summarizes the pertinent results from the design process laid out in Chapter 3 to inform the design for minimum stress RDRE combustor designs. Finally, Chapter 5 reflects on the overall objective of the research, the main takeaways, and provides suggestions for future research activities.

Chapter 2: Combustor design assumptions and boundary condition setup

This chapter discusses key assumptions which influence the combustor stress calculations. It begins by discussing the nomenclature for the combustor cooling channel geometry. Next, the applicable material properties for candidate combustor materials are established. Finally, this chapter delineates the cooling and detonation characteristics of the propellants used in the analysis described in Chapter 3.

2.1. Combustor geometry

Figure 2-1a depicts the regeneratively cooled RDRE combustor of present interest. The combustor has a total axial length of 3.81 cm and a flowpath annulus with a diameter of 7.62 cm.

Figure 2-1b is a cross-sectional view of the rectangular cooling channels which run circumferentially around the combustor. The cooling channel shape is characterized by four parameters: combustor hot wall thickness (Δ); cooling channel width (s); channel height (h); and land thickness (b). In the structural optimization framework described below, these dimensions are varied between 0.5 and 2.5 mm. The lower bound of 0.5 mm is set by the minimum wall thickness achievable with current additive manufacturing techniques.

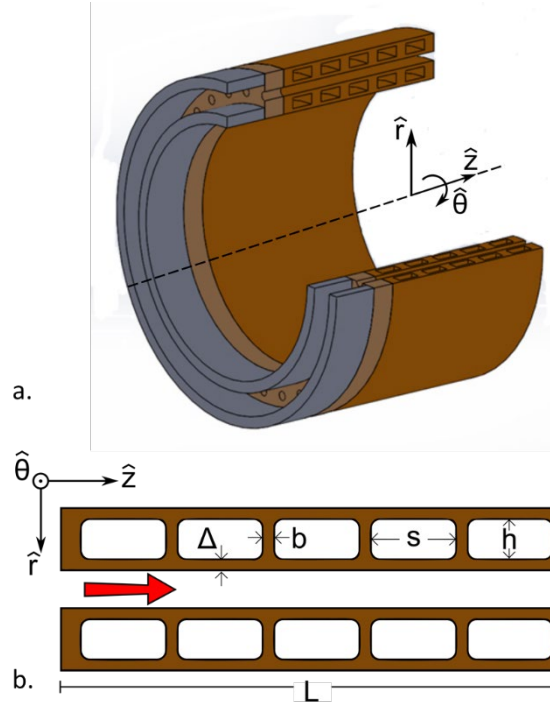


Figure 2-1: (a) Exemplary RDRE combustor. (b) Section view of cooling channels.

2.2. Combustor materials

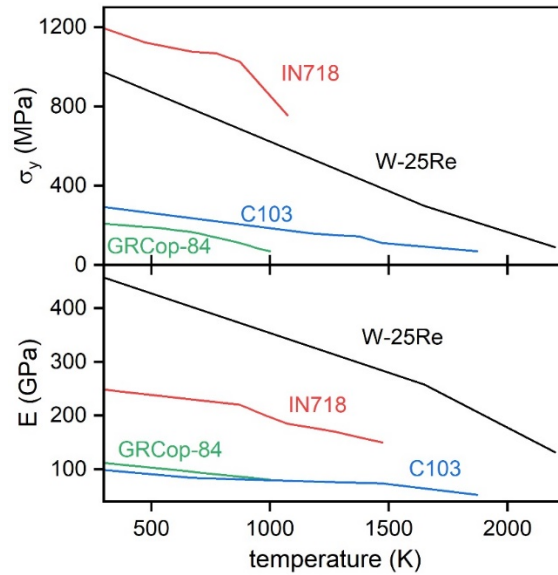
Table 2-1 summarizes the Poisson's ratio (ν), density (ρ), thermal expansion coefficient (α), thermal conductivity (κ), and maximum service temperature (T_{service}) of several candidate combustor materials: GRCo-84 [10,14,15], IN718 [16,17], Nb-C103 [18,19], W-25Re [20,21]. These materials are considered in this study because they collectively possess a wide range of properties which control the thermomechanical response of the combustor. The properties summarized in **Table 2-1** are all taken to be temperature-independent. All values correspond to room temperature measurements, except the thermal conductivity of C103, which is from 1100 K [19], and the thermal expansion coefficient and thermal conductivity of W-25Re, which are from 1600 K [20].

Table 2-1: Material properties of candidate combustor materials.

material	ν	ρ (kg/m ³)	α (10 ⁻⁶ K ⁻¹)	κ (W/m-K)	T_{service} (K)
GRCop-84 [22,27,28]	0.33 ^a	8820	19.0	304	1000
IN718 [29,30]	0.28	8220	12.8	11.4	1300
C103 [31,32]	0.40	8850	6.9	37.4	1600
W-25Re [33,34]	0.29	19700	4.5	70	2200

a. ν for C11000

The temperature-dependent 0.2% offset yield strength (σ_y) and Young's modulus (E) of the different combustor materials are presented in **Figure 2-2**. This data was aggregated from several sources [28,32,35–38]. The modulus of GRCop-84 is assumed to follow the same temperature-dependence as that of pure Cu and is estimated using the correlations in [39]. The Young's modulus of Nb-C103 is assumed to be the same as that of pure Nb, an acceptable approximation according to Titran and Klopp [40].

**Figure 2-2: Yield strength (σ_y) and Young's modulus (E) of candidate combustor materials.**

2.3. Combustion behavior

The present analysis assumes a propellant chemistry of RP-2 vapor and gaseous oxygen, premixed with an equivalence ratio of unity. This chemistry has a Chapman-Jouguet (CJ) pressure (P_{CJ}) of 2.5 MPa and a detonation velocity (V_{CJ}) of 2.4 km/s [41]. Note that the

detonation pressure, velocity, and temperature will be lower in RDREs with unmixed liquid propellants that enter the combustor through separate injectors. The time-average heat flux (q) into the hot wall is estimated using the Bartz relationship [15]:

$$q = q_0 \left(\frac{\dot{m}_f}{\dot{m}_0} \right)^{0.8}, \quad (2 - 1)$$

where \dot{m}_f is the mass flow rate of the fuel, q_0 is a reference heat flux, and \dot{m}_0 a reference mass flow rate. q_0 is set to 10 MW/m² and \dot{m}_0 to 0.5 kg/s, in line with typical values reported in the open literature [11,14,15]. According to Micka et al. [15], Eq. 2-1 predicts higher heat fluxes near the injector than are measured experimentally, meaning it gives conservative estimates of the thermal load.

2.4. Fuel properties

The thermophysical properties of the fuel used in the heat transfer and pressure drop calculations include [42–44]: density ($\rho_f = 711$ kg/m³), specific heat capacity ($C_{p,f} = 2652$ kJ/kg-K), thermal conductivity ($\kappa_f = 0.098$ W/m-K), and viscosity ($\mu = 0.00179$ Pa-s). Note that these are RP-1 properties since RP-2 data are not publicly available. The properties were averaged over the temperature range 300 to 600 K. RP-1 decomposes at temperatures above 600 K [42], limiting the maximum fuel temperature.

Chapter 3: Thermomechanical modeling

During operation of a regeneratively cooled RDRE, stresses arise from detonative loading, pressurization of the cooling channels, and thermal gradients through the combustor wall. The method for calculating each of these stress terms is outlined in this chapter using the approximation formulae summarized below. The resulting values are then superimposed and used to compute a von Mises effective stress,

$$\sigma_{VM} = \sqrt{\frac{1}{2}[(\sigma_\theta - \sigma_r)^2 + (\sigma_\theta - \sigma_z)^2 + (\sigma_r - \sigma_z)^2]}, \quad (3 - 1)$$

which is compared with σ_y of the base material to determine whether the combustor yields.

3.1. Bending stress

The hot wall experiences bending stresses due to the pressure p inside the cooling channels. The bending stresses are tensile on the hot wall outer surface and align with the axial direction. To estimate the bending stress, the hot wall is approximated as a built-in beam with span s and depth Δ subjected to a constant pressure. Accordingly, the maximum bending stress is

$$\sigma_z = \frac{1}{2}p \frac{s^2}{\Delta^2}. \quad (3 - 2)$$

Equation 3-2 agrees with 2D finite element simulations when s and Δ are smaller than 1 mm; Eq. 3-2 predicts higher stresses, and therefore gives conservative stress estimates, when s and Δ are larger than 1 mm.

3.2. Thermal stress

Non-uniform temperatures through the combustor wall result in thermal stresses. Following the approach developed by Valdevit et al. in their analysis of regeneratively cooled scramjet panels [23,24], the steady-state temperature field in the RDRE combustor is calculated using a thermal resistor network model, shown schematically in **Fig. 3-2**. The present analysis follows that of

Valdevit et al. (cf. Section III in [24]), with the modification of a fixed heat flux boundary condition (cf. Eq. 3-6) on the combustor hot wall. Per Valdevit et al. Section III [24], the system of equations can be written as,

$$\begin{cases} T_1 - T_{fuel} = q_1 r_1 + \left(q_1 + \frac{2q_{3.5,1.5}\Delta}{s} \right) r_{1.5,2} \\ T_1 - T_{fuel} = q_3 r_1 + \left(q_3 - \frac{2q_{3.5,1.5}\Delta}{b} \right) r_{3.5,4} \\ T_1 - T_{1.5} = q_1 r_1 \\ T_1 - T_{3.5} = q_3 r_1 \\ T_{3.5} - T_{1.5} = q_{3.5,1.5} r_{3.5,1.5} \end{cases} \quad (3-3)$$

In this system, the three heat fluxes, $T_{1.5}$, and $T_{3.5}$ are unknown. The heat flux terms are defined as

$$\begin{aligned} q_1 &= Q_1/s \\ q_3 &= Q_3/b \\ q_{3.5,1.5} &= Q_{3.5,1.5}/\Delta \end{aligned}, \quad (3-4)$$

and the thermal resistances are calculated using

$$\begin{aligned} r_1 &= \frac{1}{2\kappa} \Delta \\ r_{1.5,2} &= \frac{1}{2\kappa} \Delta + \frac{1}{h_f} \\ r_{3.5,4} &= \frac{1}{2\kappa} \Delta + \tanh^{-1} \left(\sqrt{\frac{2h_f}{\kappa b}} h^2 \right) \left(\sqrt{\frac{2h_f}{\kappa b}} \kappa \right)^{-1}, \\ r_{3.5,1.5} &= \frac{(s+b/2)/2}{\kappa} \end{aligned} \quad (3-5)$$

To solve the system of equations in Eq. 3-3 for the constant heat flux boundary condition and an unknown T_1 in the RDRE problem, the total heat flux q is partitioned into two components using

$$q = q_3 f_w + q_1 (1 - f_w), \quad (3-6)$$

where q_1 and q_3 are the heat fluxes into locations 1 and 3, respectively, and f_w is the line fraction of the combustor wall occupied by solid material ($b/(b+s)$). The heat transfer coefficient h_f for

the fuel coolant is calculated using a correlation for fully developed, turbulent flow through a duct [24]:

$$h_f = \frac{f}{4} \kappa_f \frac{(s+h)}{sh} \frac{(\text{Re} - 10^3) \text{Pr}}{1 + 9f^{1/2}(\text{Pr}^{2/3} - 1)}, \quad (3 - 7)$$

where the friction factor f is calculated using a correlation for turbulent flow

$$f = 7.9 \times 10^{-2} \text{Re}^{-\frac{1}{4}}, \quad (3 - 8)$$

the Reynolds number Re is

$$\text{Re} = \dot{m}_f \frac{h}{L(1 - f_w)(s+h)}, \quad (3 - 9)$$

and the Prandtl number Pr is

$$\text{Pr} = \frac{C_{p,f} \kappa_f}{\mu}. \quad (3 - 10)$$

The total mass flow rate of the fuel coolant is split evenly between the outer and inner bodies. The temperature model does not account for the curvature of either body, essentially treating them as identical flat panels.

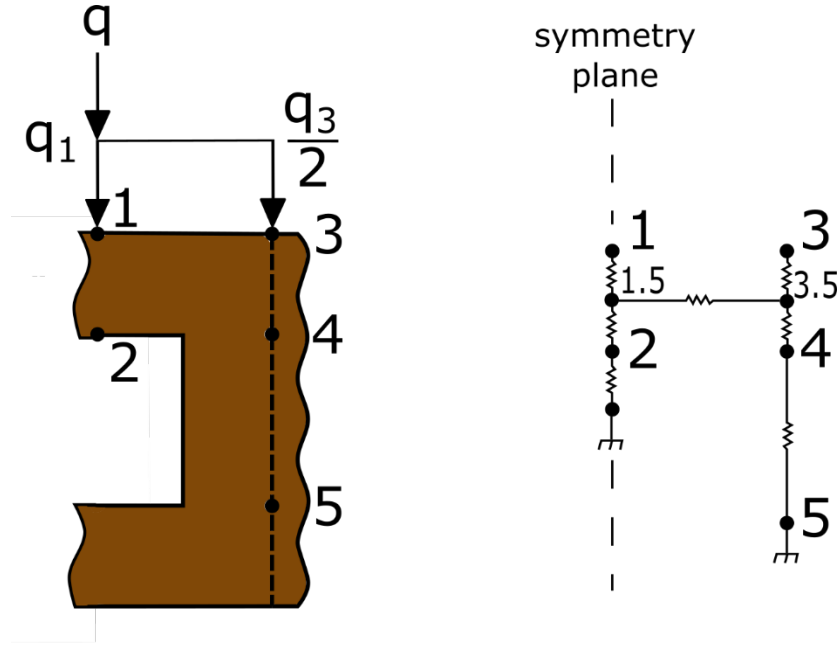


Figure 3-1: Cooling channel half unit cell with labeling to indicate nodes in thermal resistor network.

Thermal stresses arise from two sources: (1) a local temperature difference across the hot wall ($\Delta T_{local} = \frac{1}{2}[(T_1 + T_3) - (T_2 + T_4)]$) and (2) a global radial temperature difference across the entire combustor ($\Delta T_{global} = \frac{1}{2}[(T_1 + T_3) - T_5]$). The thermal stresses due to ΔT_{local} are

$$\sigma_\theta = \sigma_z = \frac{-E\alpha\Delta T_{local}}{2(1-\nu)} \quad (3-11)$$

at the hot wall surface. The thermal stresses due to ΔT_{global} are

$$\sigma_z = \frac{-E\alpha\Delta T_{global}}{2(1-\nu)}, \quad (3-12)$$

$$\sigma_\theta = \frac{-E\alpha\Delta T_{global}}{(1-\nu)} \frac{\Delta b + \Delta s + bh}{2\Delta b + 2\Delta s + bh}. \quad (3-13)$$

The geometry-dependent term in Eq. 3-13 accounts for additional stiffness due to the webbing that surrounds the cooling channels [24]. The thermal stress at the hot wall surface is compressive since the temperature there is always higher than in the rest of the combustor.

3.3. Detonative stress

To estimate the dynamic stresses due to detonative loading, the hot wall is unwrapped such that $\hat{\theta}$ is now coincident with direction \hat{x} (cf. **Fig. 3-3**). It is then approximated as a straight beam with flexural rigidity EI and linear density m subjected to a detonation wave traveling with constant velocity V_{CJ} . The coolant channels exert a restoring force on the hot wall. Thus, they are approximated as an elastic foundation with stiffness K determined by the combustor dimensions and cooling channel geometry as follows [45]

$$K = f_w \frac{L}{h} \frac{E}{1 - \nu^2}, \quad (3 - 14)$$

where L/h is the ratio of combustor length to cooling channel height. There is a mechanical analogy between a thin shell subjected to axisymmetric radial loading and a beam on an elastic foundation. Accordingly, similar to the structural response of a tube under confined detonative loading, the dynamic stresses in a beam on an elastic foundation diverge when the velocity of the moving load approaches the lowest elastic wave speed V_{Cr} of a beam on an elastic foundation, given by [46]

$$V_{Cr} = \left(\frac{4KEI}{m^2} \right)^{\frac{1}{4}}. \quad (3 - 15)$$

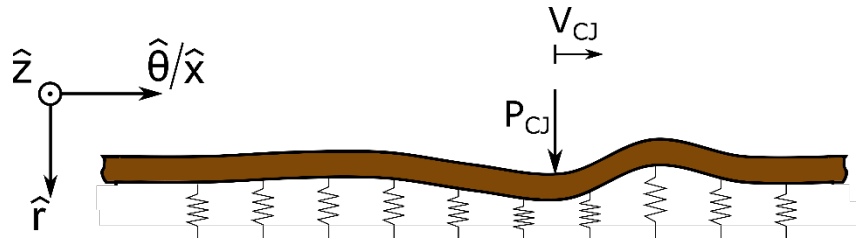


Figure 3-2: Combustor wall as a beam on an elastic foundation.

The equation of motion for surface normal deflection r of a beam on an elastic foundation under a time-dependent distributed load $P(x, t)$ is

$$P(x, t) = EI \frac{\partial^4 r}{\partial x^4} + m \frac{\partial^2 r}{\partial t^2} + Kr. \quad (3-16)$$

Kenney solved this equation in the moving frame of reference of a point load of magnitude P traveling with constant velocity V for different ranges of the ratio $\psi = V/V_{Cr}$ [46]. When $\psi > 1$, the surface displacement in the moving frame of reference of the point load is given by

$$r = \begin{cases} \frac{P\lambda}{2K} \frac{-2\sin\lambda[(\psi^2 + 1)^{1/2} - (\psi^2 - 1)^{1/2}]x}{(\psi^4 - 1)^{1/2}[(\psi^2 + 1)^{1/2} - (\psi^2 - 1)^{1/2}]} & x < 0 \\ \frac{P\lambda}{2K} \frac{-2\sin\lambda[(\psi^2 + 1)^{1/2} + (\psi^2 - 1)^{1/2}]x}{(\psi^4 - 1)^{1/2}[(\psi^2 + 1)^{1/2} + (\psi^2 - 1)^{1/2}]} & x \geq 0 \end{cases} \quad (3-17)$$

where the origin is coincident with the point load location, positive x is defined in the travel direction, and $\lambda = \left(\frac{K}{4EI}\right)^{1/4}$. When $\psi < 1$, the surface displacement is given by

$$r = \begin{cases} \frac{P\lambda}{2K} \left[\frac{e^{(1-\psi^2)\lambda x}}{1-\psi^2} \right] \left[-\frac{(1-\psi^2)^{\frac{1}{2}}}{(1+\psi^2)^{\frac{1}{2}}} \sin(1+\psi^2)^{\frac{1}{2}}\lambda\theta + \cos(1+\psi^2)^{\frac{1}{2}}\lambda x \right] & x < 0 \\ \frac{P\lambda}{2K} \left[\frac{e^{-(1-\psi^2)\lambda x}}{1-\psi^2} \right] \left[\frac{(1-\psi^2)^{\frac{1}{2}}}{(1+\psi^2)^{\frac{1}{2}}} \sin(1+\psi^2)^{\frac{1}{2}}\lambda\theta + \cos(1+\psi^2)^{\frac{1}{2}}\lambda x \right] & x \geq 0 \end{cases} \quad (3-18)$$

These solutions are extended to detonative loading in an RDRE by assuming $P = P_{CJ}L/\lambda$ and $V = V_{CJ}$. They are then used with the moment curvature relation to determine the maximum bending stress due to detonative loading:

$$\sigma_\theta = -\frac{1}{2}E\Delta \frac{d^2 r}{dx^2}. \quad (3-19)$$

The maximum stress on the hot wall due to detonative loading is always compressive.

3.4. Regenerative cooling considerations

At the entrance to the regenerative cooling channels, the fuel is assumed to have an inlet temperature (T_i) of 300K and an inlet pressure of 15 MPa. There are two constraints on the regenerative cooling behavior: (i) the fuel temperature T_f must not exceed the decomposition limit of 600K [30], and (ii) the total pressure drop Δp across the coolant channels must not exceed a certain limit. Here the maximum allowable pressure drop is 1.5 MPa, in line with typical values in conventionally regenerative cooled combustors [47]. Following Valdevit et al. [24], the fuel temperature at the channel outlet (T_f) is

$$T_f = T_i + \frac{2hL(1 - f_w)}{\dot{m}_f} \frac{q}{C_{p,f}} \frac{\pi(D - \Delta)}{(b + s)}, \quad (3 - 20)$$

where the total circumferential length of the cooling channel is $\pi(D - \Delta)$. T_f is used in the temperature constraint on the fuel and also in the combustor heat transfer calculations to determine the maximum hot wall temperature, while T_i is used in the thermal stress calculations. Following Kanda et al. [47] the pressure drop across the length of the cooling channel is

$$\Delta p = \frac{1}{\rho_f} \frac{f}{2} \frac{(s + h)}{2sh} \left(\frac{\dot{m}_f}{2h(1 - f_w)} \right)^2. \quad (3 - 21)$$

Chapter 4: Results and discussion

This chapter presents the results from the implementation of the methodology and assumptions outlined in the previous two chapters. These results consist of an example combustor design map, a set of summary plots for visualizing the optimization results, geometry for optimized designs at various mass flow rates, the corresponding impact on weight based on this geometry, and the impact of dynamic resonance on RDRE combustor design. These results enable the designer to visualize the design space and inform the design of an actively cooled RDRE.

Figure 4-1a is a cooling channel design map for a GRCo-84 RDRE combustor with fixed cooling channel height $h = 0.5$ mm, land thickness $b = 1$ mm, and fuel flow rate $\dot{m}_f = 1.0$ kg/s. The axes of hot wall thickness Δ and channel width s span ranges of 0.5 to 1.5 mm and 0.5 to 2.5 mm, respectively. Note that this representation is a 2D view of the 4D cooling channel parameter space. The iso-contours show the ratio of the von Mises effective stress σ_{VM} , calculated using the formulae in Chapter 3, to the temperature-dependent yield strength. Combinations of Δ and s for which $\sigma_{VM}/\sigma_y < 1$ avoid plastic yielding, although the cooling channels might exhibit time-dependent deformation (i.e. creep), an effect not considered here but likely important in practice. The red contour denotes designs for which $\Delta p = 1.5$ MPa; combinations of Δ and s above this contour have a lower pressure drop, thus satisfying the constraint $\Delta p < 1.5$ MPa. The normalized stress iso-contours show that thin channels and a thin hot wall minimize σ_{VM}/σ_y ; however, the Δp constraint prevents the channel width from becoming too thin. The regions highlighted in green correspond to designs which satisfy the constraints on pressure drop ($\Delta p < 1.5$ MPa), fuel temperature ($T_f < 600$ K), and metal temperature ($T_{max} < T_{service}$). Within these regions, the parameters $\Delta = 0.54$ mm and $s = 1.55$ mm (indicated by the filled marker) minimize the stress ratio, meaning this set of geometric parameters should maximize combustor longevity. Importantly, the stresses diverge for designs in which the detonation velocity matches the elastic wave speed of the combustor wall, predicted using the elastically supported beam approximation. This critical condition, denoted by the contour labeled $V_{Cr} = V_{CJ}$, splits the region of viable designs in **Fig. 4-1a**. **Fig. 4-1b** shows normalized von Mises, thermal, bending, and dynamic stresses plotted against the hot wall thickness Δ for designs that lie along the broken horizontal line in **Fig. 4-1a**. Thermal stress dominates most of the design space, although bending stress

becomes important as the hot wall thickness approaches 0.5 mm. Again, dynamic stresses diverge near $\Delta = 0.7$ mm, when $V_{Cr} = V_{CJ}$.

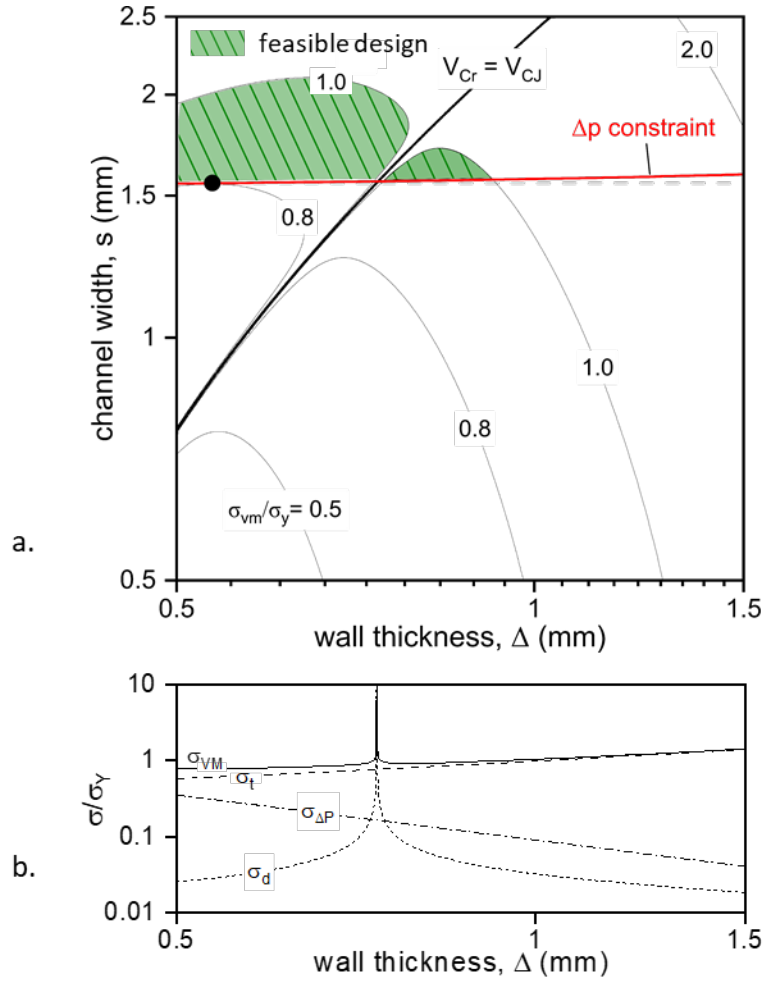


Figure 4-1: (a) Design map for regeneratively cooled GRCop-84 RDRE combustors with iso-contours of constant σ_{VM}/σ_y . Fixed parameters include: $h = 0.5$ mm, $b = 1$ mm, and $\dot{m}_f = 1$ kg/s. The red contour denotes designs for which $\Delta p = 1.5$ MPa. Viable designs which satisfy the different design and performance constraints are highlighted green. The filled marker indicates the optimal design which minimizes stress σ_{VM}/σ_y . (b) von Mises, thermal, bending, and dynamic stresses plotted against hot wall thickness for the same conditions as in (a), with the additional constraint $s = 1.55$ mm.

Figure 4-2 displays cooling channel designs which minimize the normalized effective stress (σ_{VM}/σ_y) at a given mass flow rate while satisfying constraints on pressure drop ($\Delta p < 1.5$ MPa), fuel temperature ($T_f < 600$ K), and metal temperature ($T_{max} < T_{service}$). By minimizing σ_{VM}/σ_y , these designs are expected to maximize combustor longevity. For each

material, the data terminate at the maximum feasible fuel flow rate, above which there are no viable designs. The maximum flow rates are 0.21, 0.56, 1.95, and 2.00 kg/s for IN718, Nb-C103, GRCo-84, and W-25Re, respectively. To minimize thermal stress, the optimal hot wall thickness remains near 0.5 mm, the lower bound, for all materials over the full range of mass flow rates. The other geometric parameters vary with increasing mass flow rate, with distinct trends seen in each material. The low thermal conductivity of IN718 results in high thermal stresses and yielding at relatively low mass flow rates. For Nb-C103, the optimal designs evolve towards short, narrow cooling channels with increasing mass flow rate to increase the fuel velocity and, as a result, the heat transfer coefficient. For GRCo-84, which has an exceptionally high thermal conductivity, the optimal designs trend towards tall, thin coolant channels with thick webbing to maximize heat conduction from the hot wall surface while minimizing bending stresses. Lastly, for W-25Re, which possesses high strength at elevated temperatures, the optimal designs at high mass flow rates feature shorter, wider channels. The data for Nb-C103, GRCo-84 and W-25Re all contain numerical noise. Additionally, there are distinct jumps in the optimal design parameters at certain mass flow rates (e.g., 0.24 kg/s for GRCo-84) to avoid the condition $V_{Cr} = V_{CJ}$ and resulting high dynamic stresses.

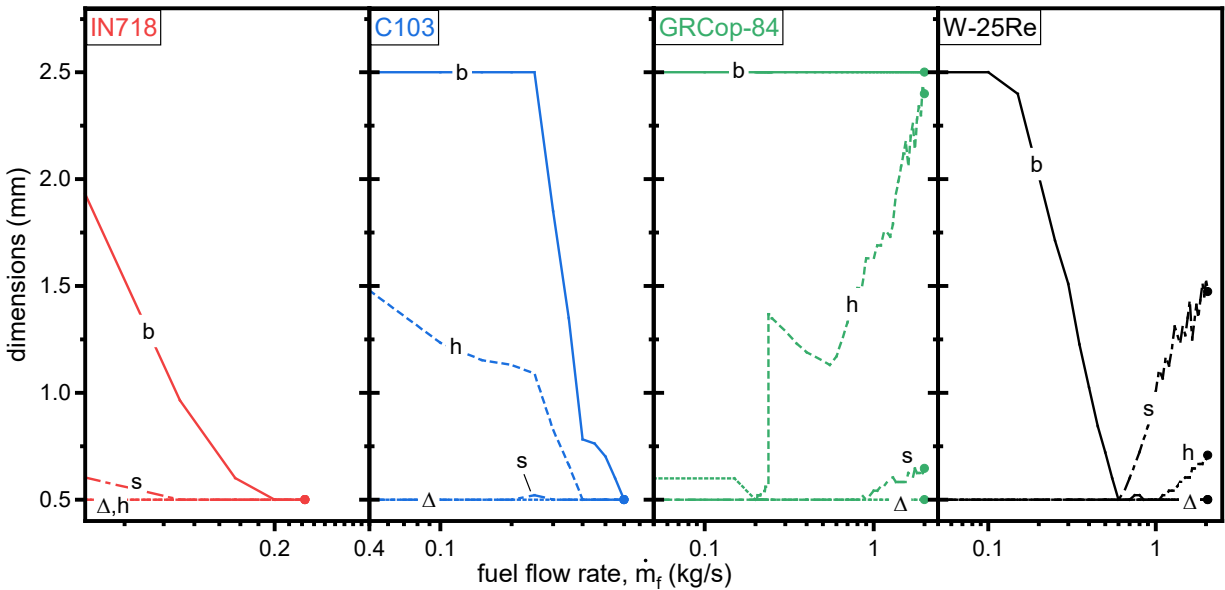


Figure 4-2: Cooling channel dimensions which minimize normalized effective stress (σ_{VM}/σ_y) at a given mass flow rate while satisfying constraints on pressure drop ($\Delta p < 1.5 \text{ MPa}$), fuel temperature ($T_f < 600 \text{ K}$), and metal temperature ($T_{max} < T_{service}$).

Figure 4-3 shows constraint activity parameters, defined as a parameter normalized by its limiting value specified in a design constraint, as a function of fuel flow rate for the optimal cooling channel designs summarized in **Fig. 4-3**. The constraint activity parameters range from 0 to an upper limit of unity when the constraint is identically satisfied. In the present optimization study, there are constraint activity parameters for stress $\tilde{\Sigma}$ (σ_{VM}/σ_y); cooling channel dimensions \tilde{L} (Δ_{\min}/Δ , b_{\min}/b); temperature \tilde{T} ($T_f/T_{f,\max}$, $T_{\max}/T_{\text{service}}$); and coolant pressure drop $\tilde{\Delta P}$ ($\Delta p/\Delta p_{\max}$). In **Fig. 4-3** the $\tilde{\Sigma}$ data again highlight that thermal stress dominates the design space over the full range of fuel flow rates. Onset of plastic yielding due to thermal stresses ultimately determines the maximum fuel flow rate. As noted above, for all materials, the hot wall thickness remains near its limiting value of 0.5 mm. Additionally, with the exception of GRCo-84, the land thickness approaches its lower limit of 0.5 mm near the maximum fuel flow rate to minimize the transverse thermal resistance. The maximum temperatures of the fuel and the hot wall surface are both well below their corresponding limits for all materials. Lastly, for GRCo-84, Nb-C103, and W-25Re, the pressure drop remains near its upper bound at the highest fuel flow rates, thus maximizing the coolant velocity and the heat transfer coefficient.

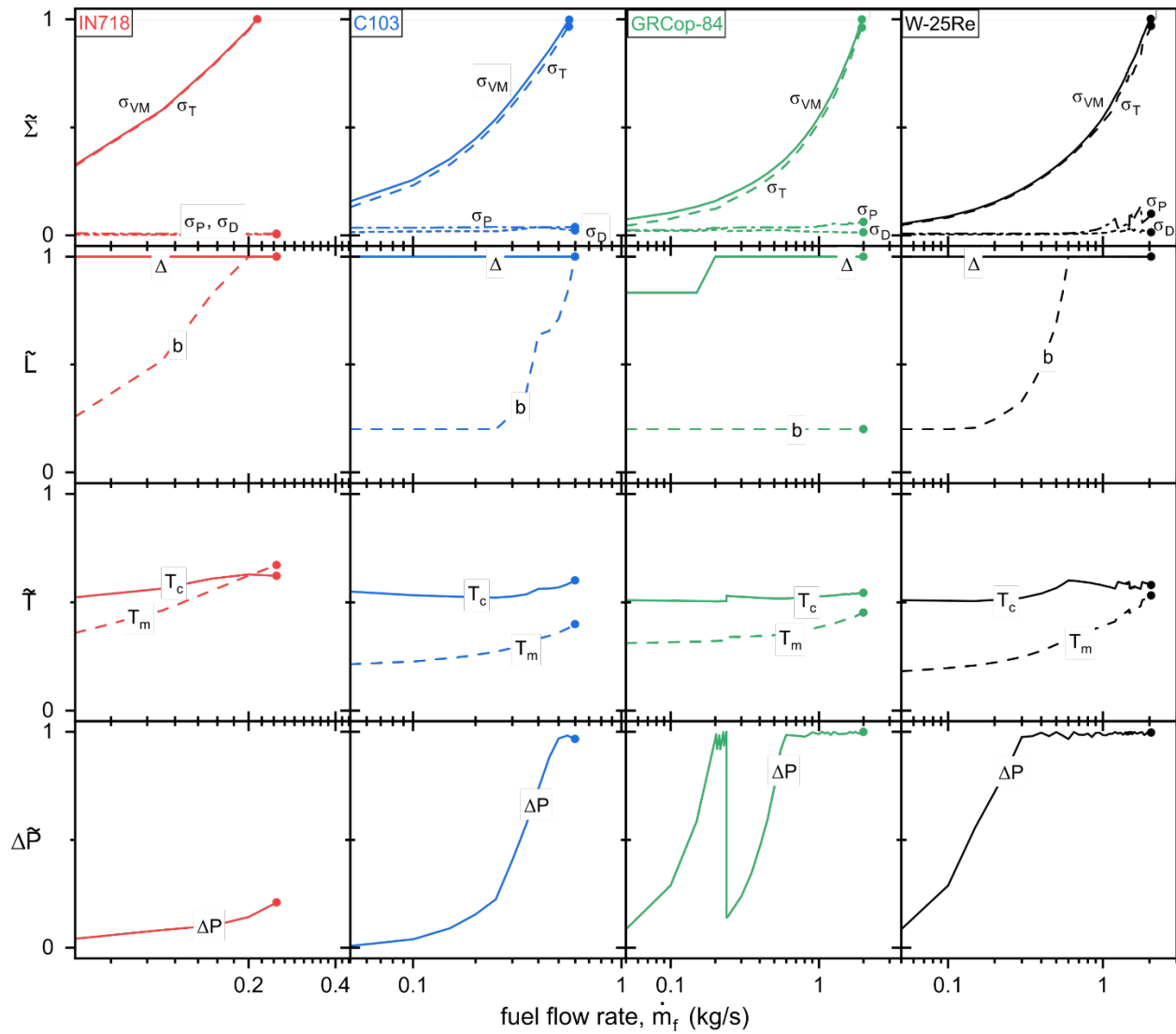


Figure 4-3: Constraint activity parameters vs. fuel flow rate for optimal cooling channel configurations in Fig. 4-2.

Figure 4-4 compares the areal density of the optimal combustor designs for each material, where areal density is defined as the total combustor mass normalized by its projected area in the r - θ plane. Note that the trends in **Fig. 4-4** would change if the objective function sought minimal mass designs instead of designs which minimize σ_{VM}/σ_y . Nevertheless, optimizing for longevity shows that at low mass flow rates, IN718 yields the lightest combustors owing to its high specific strength. For intermediate mass flow rates, Nb-C103 combustors have the lowest areal density. Finally, at the highest flow rates, W-25Re combustors have the lowest areal density, despite W-25Re being almost three times more dense than GRCop-84. This surprising behavior

results because GRCop-84 minimizes thermal stresses via tall cooling channels, which increase the combustor mass.

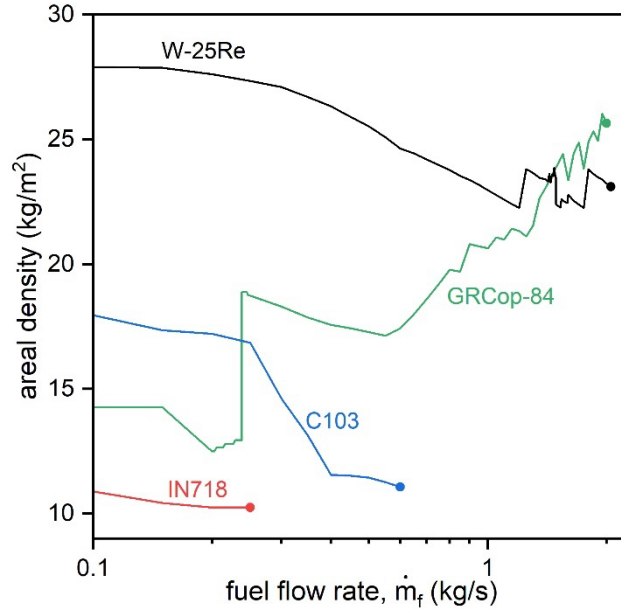


Figure 4-4: Areal density of optimal combustor designs vs. fuel flow rate.

To highlight the important role of dynamic stresses in structural optimization of RDRE combustors, **Fig. 4-5** compares the ratio of the CJ velocity to the elastic wave speed to the (i.e., V_{CJ}/V_{Cr}) for combustor designs which minimize static stresses only vs. designs which minimize both static and dynamic stresses. Detonative loads have only a weak effect on the structural optimization of IN718 combustors since designs with low static stresses also avoid the condition $V_{Cr} = V_{CJ}$. By contrast, minimizing only static stresses in Nb-C103, W-25Re, or GRCop-84 combustors yields designs for which $V_{Cr} = V_{CJ}$ and dynamic stresses diverge. Thus, correctly accounting for dynamic stresses is critically important with these materials. When dynamic stresses are taken into account, Nb-C103 combustor designs have an elastic wave speed smaller than V_{CJ} over the full range of mass flow rates. W-25Re and GRCop-84 combustors transition from $V_{Cr} > V_{CJ}$ at low mass flow rates to $V_{Cr} < V_{CJ}$ at high mass flow rate; there is a discrete jump in the elastic wave speed at the transition between these two regimes.

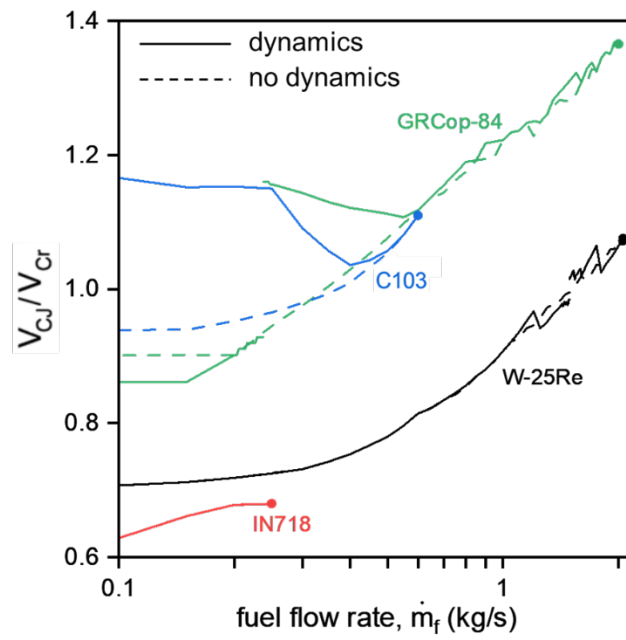


Figure 4-5: V_{CJ}/V_{Cr} versus fuel flow rate for different combustor materials. Note Nb-C103, W-25Re, GRCop-84 combustors all avoid the critical condition, $V_{Cr} = V_{CJ}$, when dynamic stresses are considered.

Chapter 5: Conclusions

A framework has been developed to determine regeneratively cooled RP2/GOX RDRE combustor designs which minimize static and dynamic stresses while satisfying constraints on maximum coolant temperature, maximum hot wall surface temperature, and coolant pressure drop. By minimizing the deviatoric stress, these designs should maximize combustor longevity. The framework was used to determine optimal designs for the candidate combustor materials GRCop-84, IN718, W-25Re, and Nb-C103.

5.1. Combustor design key results

The key results are as follows:

1. Each material has a maximum feasible fuel flow rate, above which the material starts to plastically deform. The maximum flow rates range from 0.21 kg/s for IN718 to 2.00 kg/s for W-25Re. Note that although the magnitudes of these flow rates may change with overall combustor dimensions and propellant chemistry, the relative ranking of the different materials will likely remain the same.
2. Thermal stresses dominate the design space for each material, although dynamic stresses from confined detonative loading become important under certain conditions. The optimal designs minimize thermal stresses with thin hot walls and by improving heat transfer from the hot wall surface, either through higher heat transfer coefficients into the fuel coolant or, in the case of high thermal conductivity GRCop-84, thicker webbing between the individual coolant channels. The channels tend to constrict the flow in order to increase the coolant velocity and the heat transfer coefficient. An important consequence is that designs often evolve towards configurations which just satisfy the pressure drop constraint.
3. Dynamic stresses become significant when the detonation wave speed approaches the elastic wave speed of the combustor hot wall, predicted using an elastically supported beam approximation. In GRCop-84, Nb-C103, and W-25Re combustors, channel designs which only minimize thermal and bending stresses can sometimes amplify the dynamic stresses. Thus, it is critically important to consider dynamic stress effects when designing RDRE combustors from these materials.

5.2. Future work

The research presented in this paper is a key step toward enabling the prolonged operation of RDREs. The following should be considered to further the state-of-the-art in RDRE development:

1. The calculations performed in this thesis are based on CJ detonation parameters resulting from a pre-vaporized RP2/GOX detonation reaction with an equivalence ratio of 1.0. However, varying the equivalence ratio can be useful for optimizing engine cycle performance, controlling the composition of combustion byproducts, etc. Bennewitz et al. performed detonation parameter calculations at various equivalence ratios [41]. **Figure 5-1** shows a subset of these results from a 0.75 to 1.75 equivalence ratio. The pressure and velocity changes will have a direct impact on the dynamic loading. However, the Bartz equation used to scale the heat flux based on mass flow rate of fuel does not capture effects of varying equivalence ratio. It remains to be seen whether the equivalence ratio influences the heat flux which is the main driver of stresses RDREs. Determining this relationship between equivalence ratio and heat flux would improve the modeling capability for this design problem.

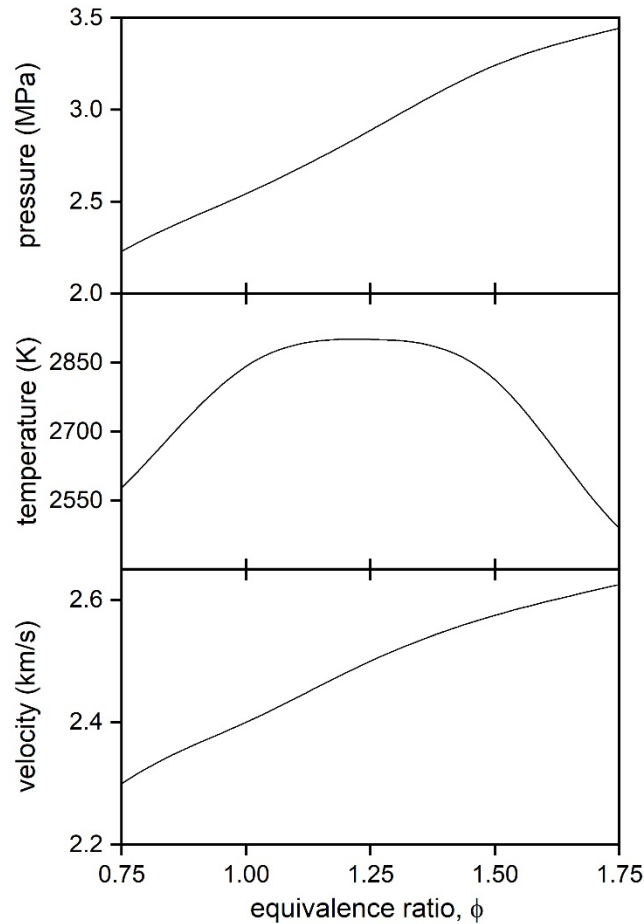


Figure 5-1: Chapman-Jouguet parameters for a pre-vaporized RP2/GOX detonation reaction as functions of equivalence ratio ϕ .

2. In the context of this paper, maximizing the life of an RDRE combustor was equivalent to minimizing the yield stress ratio. Although this value was used to represent a first order estimate of material capability, further work should be conducted to refine how the loading environment will impact the life of the combustor. Beyond just the yield strength of the material, the other failure modes that should at least be considered are creep, low cycle fatigue, high cycle fatigue, and strain ratcheting. Examining these in greater detail will enable refined estimates of combustor life.
3. Lastly, a comprehensive experimental study should be conducted to validate the beam on an elastic foundation model approach to predicting the presence of dynamic stress amplification in actively cooled RDRE combustors.

Appendix

This appendix section contains the scripts used to run the optimization described in this paper. Matlab R2018b was used for this analysis. The main script calls upon four separate functions, all of which are included here.

Run script:

```
% Eric Jorgensen, MIT 2021, Master's thesis RDRE combustor optimization

clear all

clc

% material flag to set material properties, 1 is GRCo-84, 2 is IN718, 3 is
% Nb C103, 4 is W25Re
material=1;

% set vectors of fuel flow rate, channel height, channel support thickness,
% hot wall thickness, and channel width to sweep through in the
% optimization
mdot_f_vec=linspace(0.05,2.0,5);

h_vec=linspace(0.0005,.0025,5);
b_width_vec=linspace(0.0005,.0025,5);
t_vec=linspace(0.0005,.0025,5);
channel_width_vec=linspace(0.0005,.0025,5);

% preallocate output matrix to be filled in with function calculations
% based on the number of geometric variations to sweep through
config_len=length(h_vec)*length(b_width_vec)*length(t_vec)*length(channel_wid-
th_vec);
config_mat=zeros(13,config_len);

% loop through all the different geometric combinations at all the fuel
% flow rates and allocate them to a column in the output matrix
for hh = 1:length(mdot_f_vec)
    mdot_f=mdot_f_vec(hh);
    for dd = 1:length(channel_width_vec)
        for cc = 1:length(t_vec)
            for bb = 1:length(b_width_vec)
                for aa = 1:length(h_vec)
                    config_mat(1,(aa+(bb-1)*length(h_vec)+(cc-
1)*length(b_width_vec)*length(h_vec)+(dd-
1)*length(b_width_vec)*length(h_vec)*length(t_vec)))=h_vec(aa);
                    config_mat(2,(aa+(bb-1)*length(h_vec)+(cc-
1)*length(b_width_vec)*length(h_vec)+(dd-
1)*length(b_width_vec)*length(h_vec)*length(t_vec)))=b_width_vec(bb);
                    config_mat(3,(aa+(bb-1)*length(h_vec)+(cc-
1)*length(b_width_vec)*length(h_vec)+(dd-
1)*length(b_width_vec)*length(h_vec)*length(t_vec)))=t_vec(cc);
```

```

        config_mat(4, (aa+(bb-1)*length(h_vec)+(cc-
1)*length(b_width_vec)*length(h_vec)+(dd-
1)*length(b_width_vec)*length(h_vec)*length(t_vec)))=channel_width_vec(dd);
    end
end
end

% assigns the geometric parameters from the output matrix from a given
% column to pass to the function that will run the temperature
% calculations for the full length of the cooling channel to check the
% pressure drop and temperature constraints
for ee = 1:config_len
    h = config_mat(1,ee);
    b = config_mat(2,ee);
    t = config_mat(3,ee);
    s = config_mat(4,ee);
    [config_mat(5,ee), config_mat(6,ee), config_mat(7,ee),
config_mat(8,ee)] = config_check_R2_fn(material, h, b, t, s, mdot_f);

    % checking the output from the config check function for metal
    % temperature, fuel temperature, pressure drop, and reynolds number
    % to make sure the turbulent flow assumption remains valid. All the
    % constraints are normalized by their limit factors
    if material == 1
        config_mat(5,ee)=config_mat(5,ee)/1000;
        config_mat(6,ee)=config_mat(6,ee)/600;
        config_mat(7,ee)=config_mat(7,ee)/1.5;
        config_mat(8,ee)=config_mat(8,ee)/4000;
    elseif material == 2
        config_mat(5,ee)=config_mat(5,ee)/1300;
        config_mat(6,ee)=config_mat(6,ee)/600;
        config_mat(7,ee)=config_mat(7,ee)/1.5;
        config_mat(8,ee)=config_mat(8,ee)/4000;
    elseif material == 3
        config_mat(5,ee)=config_mat(5,ee)/1600;
        config_mat(6,ee)=config_mat(6,ee)/600;
        config_mat(7,ee)=config_mat(7,ee)/1.5;
        config_mat(8,ee)=config_mat(8,ee)/4000;
    elseif material == 4
        config_mat(5,ee)=config_mat(5,ee)/2200;
        config_mat(6,ee)=config_mat(6,ee)/600;
        config_mat(7,ee)=config_mat(7,ee)/1.5;
        config_mat(8,ee)=config_mat(8,ee)/4000;
    end
end

% re-runs temperatures based on inlet of the cooling channel since
% thermal gradients are highest there, calculates stress from cooling
% channel pressurization, and runs a function to calculate the dynamic
% stresses for each design configuration
for ff = 1:config_len
    h = config_mat(1,ff);
    b = config_mat(2,ff);
    t = config_mat(3,ff);
    s = config_mat(4,ff);

```

```

        [config_mat(9,ff), config_mat(10,ff), config_mat(11,ff),
config_mat(12,ff), config_mat(13,ff)] = wall_temp_sweeps_R6_fn(material, h,
b, t, s, mdot_f);
    end

    % since the constraints are all normalized to 1.0, anything equal to or
    % greater than 1.0 is beyond the constraint and therefore filtered out
    for gg = 1:config_len
        if config_mat(5,gg) >= 1.0
            config_mat(9,gg) = Inf;
        end
        if config_mat(6,gg) >= 1.0
            config_mat(9,gg) = Inf;
        end
        if config_mat(7,gg) >= 1.0
            config_mat(9,gg) = Inf;
        end
        if config_mat(8,gg) <= 1.0
            config_mat(9,gg) = Inf;
        end
    end
end

% identifies the column with the minimum von Mises stress ratio, this
% column is then used to extract all the geometric parameters
% associated with the minimum stress design for a given fuel flow rate,
% subject to the imposed constraints above
min_stress = min(config_mat(9,:));
[x,y]=find(config_mat==min_stress);

stress_vec_final(hh) = config_mat(9,y);
therm_vec_final(hh) = config_mat(10,y);
delP_vec_final(hh) = config_mat(11,y);
dyn_vec_final(hh) = config_mat(12,y);
h_final(hh) = config_mat(1,y);
b_final(hh) = config_mat(2,y);
t_final(hh) = config_mat(3,y);
s_final(hh) = config_mat(4,y);
met_temp_final(hh) = config_mat(5,y);
fuel_temp_final(hh) = config_mat(6,y);
delP_final(hh) = config_mat(7,y);
vr(hh) = config_mat(13,y);
end

```

function “wall_temp_sweeps_R6_fn” called in the main run script:

```

function [M, M1, M2, M3, vr] = wall_temp_sweeps_R6_fn(material, h, b, t, s,
mdot_f)

% Eric Jorgensen, MIT 2021, Master's thesis RDRE combustor optimization

% sets the internal channel pressure
P_o=15;

% sets the equivalence ratio of the combustion reaction
eq = 1;

```

```

% sets the material properties based on the flag passed for material
if material == 1
    k = 304;
    vs=0.33;
    rho=8820;
    alpha = 1.90e-05;
elseif material == 2
    k = 11.4;
    vs = 0.284;
    rho = 8220;
    alpha = 1.28e-05;
elseif material == 3
    k = 37.4;
    vs = 0.397;
    rho = 8850;
    alpha = 6.9e-06;
elseif material == 4
    k = 70;
    vs = 0.29;
    rho = 19700;
    alpha = 4.5e-06;
end

% look up tables for pressure ratio and CJ velocity based on varying
% equivalence ratio for RP2-GOX detonation reaction
eq_ratio=[0.25,0.5,0.75,1,1.25,1.5,1.75,2,2.25,2.5,2.75,3];
p_ratio=[12.5,17.5,22,25.1,28.5,32,34,35.5,36,35.5,34,32];
cj_vel=[1800,2100,2300,2400,2500,2575,2625,2650,2600,2575,2525,2425];

P_det = interp1(eq_ratio,p_ratio,eq,'linear','extrap');
Vcj = interp1(eq_ratio,cj_vel,eq,'linear','extrap');

% reference mdot_f and heat flux to use in bartz equation scaling. this
% ties the input fuel flow rate to the heat flux in the temperature
% calculations
mdot_ref = 0.5; % kg/s
q_ref = 10e6; % W/m^2

% coolant properties for RP-1, density and inlet/outlet temps of ~300 and
% 600K, average viscosity over that range, average thermal conductivity
% over that range. inlet coolant temp, average specific heat over
% temperature range
rho_c_1 = 805;
rho_c_2 = 587;
mu = 5.64684E-05;
k_c = 0.077918;
Tc_in = 293+0;
Cp_1 = 2651;
Pran = Cp_1*mu/k_c;

% combustor axial length
L_comb=0.0254*1.5;

%det PR * atmospheric pressure (to calc actual pressure)

```

```

% then * axial length to get N/m, input to dynamics calc
P1 = P_det*L_comb*101325;

% calculate q value based on Bartz scaling relationship
q = q_ref * (2*(mdot_f/2)/mdot_ref)^(0.8);

% based on the channel spacing and channel support width, the number of
% discrete channels is calculated and channel characteristic dimensions
% such as hydraulic diameter
A_sect=h*L_comb;
n_cell=L_comb/(b+s);
A_rat=(b*n_cell)/((b+s)*n_cell);
A_flow_c = A_sect*(1-A_rat);
channel_arc_OD = L_comb*(1-A_rat)/n_cell;
channel_arc_ID = channel_arc_OD;
cooling_channel_area = A_flow_c/n_cell;
cooling_channel_perim = channel_arc_OD+channel_arc_ID+2*h;
d_h = 4*cooling_channel_area/cooling_channel_perim;

% for the outer body, the length of the channel is based on the
% flowpath/hotwall diameter plus the thickness of the hot wall, dividing by
% 100 to capture inlet effects.
L_channel=2*pi*((.0381+t)/100);

% flow velocity is calculated based on m_dot = rho*V*A relationship. area
% is established above, derived from channel height, channel width, and
% channel support width. mdot_f is divided by 2 here since half the fuel
% flow would be used to cool the outer body and half would be used for the
% center body
v_c = (mdot_f/2)/((rho_c_1+rho_c_2)*A_flow_c);

% Reynolds number, friction factor, and convective heat transfer coefficient
% is calculated based on turbulent flow through pipe equations/correlations
Re_d = ((rho_c_1+rho_c_2)/2*v_c*d_h)/mu;
fric = 0.0791*(Re_d)^(-1/4);
h_c = k_c/d_h*((fric/2)*(Re_d-1000)*Pran)/(1+12.7*sqrt(fric/2)*(Pran^(2/3)-1));

% thermal resistance values calculated based on equations from Valdevit "A
% materials selection protocol for lightweight actively cooled panels"
r_1 = 1/2*(t/k);
r_2w = 1/2*(t/k)+1/h_c;
r_h = ((channel_arc_ID+b/2)/2)/k;
r_2c = 1/2*(t/k)+(atanh(sqrt((2*h_c)/(k*b)*h^2)))*(sqrt(2*h_c/(k*b))*k)^(-1);

% fuel temperature equation
T_fuel =
(q*L_channel)/((rho_c_1+rho_c_2)/2*Cp_1*v_c*(b+channel_arc_ID))+Tc_in;

% setting up systems of equation for linear system solve, added fixed
% heatflux BC, otherwise same as Valdevit system
A = [-1 0 0 (2*t*r_2w/channel_arc_ID) 0 (r_1+r_2w); -1 0 0 (-2*t*r_2c/b)
(r_1+r_2c) 0; 1 -1 0 0 0 -r_1; 1 0 -1 0 -r_1 0; 0 -1 1 -r_h 0 0; 0 0 0 0 b
channel_arc_ID];

```

```

b_rhs = [-T_fuel; -T_fuel; 0; 0; 0; q*(b+channel_arc_ID)];

x = linsolve(A,b_rhs);

% mechanical stresses from internal channel pressurization
sig_ax_p0_mat_om = ((s/t)^2/2)*P_o*10^6;
sig_circ_p0_mat_om = vs*sig_ax_p0_mat_om;

% rename variables from linear system solve above
q_h_sol = x(4);
q_w_sol = x(6);
q_c_sol = x(5);
T_wtf_sol = x(2);
T_ctf_sol = x(3);
T_m_channel_out = x(1); % Loc 1

% using temperatures and heat fluxes solved above, calculate temperatures
% at the stations of interest throughout the cooling channel unit cell
T_m_channel_in = T_wtf_sol-(q_w_sol+2*(q_h_sol)*t/channel_arc_ID)*(t/2)/k; %
Loc 2
T_m_side_in = T_ctf_sol-(q_c_sol/2-2*(q_h_sol)*t/b)*(t/2)/k; % Loc 4
T_m_side_out = T_ctf_sol+(q_w_sol*(t/2)/k); % Loc 3
T_m_cool = T_m_side_in-(q_c_sol/2-2*(q_h_sol)*t/b)*(r_2c-1/2*(t/k)); %Loc 5

% temp for dynamic stresses based on average temp across full channel
global_avg_temp = double((T_m_channel_out+T_m_cool)/2);

avg_outer_wall_temp = (T_m_channel_out+T_m_side_out)/2;
avg_inner_wall_temp = (T_m_channel_in+T_m_side_in)/2;
local_avg_temp = (avg_outer_wall_temp+avg_inner_wall_temp)/2;
global_avg_temp = double((T_m_channel_out+T_m_cool)/2);

af_mat = t*(channel_arc_OD+b);
ac_mat = b*(h);

% filter out design configurations where r_2c value becomes imaginary. r_2c
% varies (approximately) linearly with fuel flow rate. this relationship
% was calculated using linear regression and used to smooth out noise
% caused by imaginary number for the output plots
real_check = isreal(r_2c);
if (real_check == 0)
    vr = Inf;
    M = Inf;
    M1 = Inf;
    M2 = Inf;
    M3 = Inf;
elseif (real_check == 1)
    % determines modulus and yield strength value of the material based
    % on the average temperature and its material flag, getProperty
    % function has look up tables based on material
    [E_avg] = getProperty(global_avg_temp, material);
    [E_mat_outer, YS_mat_outer] = getProperty(avg_outer_wall_temp, material);
    [E_mat_avg, YS_mat_avg] = getProperty(avg_inner_wall_temp, material);
    % dynamic stress value and velocity ratio computed in calcDynamic
    % function, based on geometric parameters and detonation

```



```

    % characteristics
    [dynamic_stress, vr] = calcDynamic(vs, E_avg, t, h, L_comb, A_rat, rho,
P1, Vcj);

    % averaging the hot wall, cooling channel outer wall temps for use in
    % stress calculations
    global_deltT_map=((T_m_channel_out-T_m_cool)+(T_m_side_out-T_m_cool))/2;
    local_deltT_map=((T_m_side_out-T_m_side_in)+(T_m_channel_out-
T_m_channel_in))/2;

    % thermal stress calculations based on Valdevit et al. expressions in
    % "Design of actively cooled panels for scramjets"
    sig_ax_tg_om = -alpha*E_mat_avg.*global_deltT_map/(2*(1-vs));
    sig_circ_tg_om = -alpha*E_mat_avg.*global_deltT_map.*(af_mat+ac_mat)./(1-
vs)*(2*af_mat+ac_mat));
    sig_ax_tL_om = -alpha*E_mat_avg.*local_deltT_map/(2*(1-vs));
    sig_circ_tL_om = -alpha*E_mat_avg.*local_deltT_map/(2*(1-vs));

    % renamed dynamic stresses from calcDynamic function
    sig_ax_dyn_om = -dynamic_stress;

    % von Mises stress, thermal contributions only
    sig_vm_dt_om = sqrt(1/2.*(((sig_ax_tg_om+sig_ax_tL_om)-
(sig_circ_tg_om+sig_circ_tL_om)).^2+((sig_circ_tg_om+sig_circ_tL_om)-
0).^2+(0-(sig_ax_tg_om+sig_ax_tL_om)).^2)));

    % von Mises stress, channel pressurization contributions only
    sig_vm_p0_om = sqrt(1/2.*((sig_ax_p0_mat_om-
sig_circ_p0_mat_om).^2+(sig_circ_p0_mat_om-0).^2+(0-sig_ax_p0_mat_om).^2));

    % von Mises stress, combined
    sig_vm_comb_om =
sqrt(1/2.*(((sig_ax_tg_om+sig_ax_tL_om)+sig_ax_p0_mat_om+sig_ax_dyn_om)-
(sig_circ_p0_mat_om+(sig_circ_tg_om+sig_circ_tL_om))).^2+((sig_circ_p0_mat_om
+(sig_circ_tg_om+sig_circ_tL_om))-0).^2+((0-
(sig_ax_tg_om+sig_ax_tL_om)+sig_ax_p0_mat_om+sig_ax_dyn_om)).^2));

    % renamed VM yield stress ratios for function output
    M = sig_vm_comb_om./YS_mat_outer;
    M1 = sig_vm_dt_om./YS_mat_outer;
    M2 = sig_vm_p0_om./YS_mat_outer;
    M3 = abs(sig_ax_dyn_om)./YS_mat_outer;
end
end

```

function “getProperty” called within the “wall_temp_sweeps_R6_fn” function:

```

function [E, YS] = getProperty(temp, material)

% Eric Jorgensen, MIT 2021, Master's thesis RDRE combustor optimization

if material == 1
temp_grc = [270, 300, 350, 400, 450, 500, 550, 600, 650, 700, 750, 800, 850,
900, 950, 1000];

```

```

ys_grc = [208e6, 208e6, 203e6, 199e6, 194e6, 190e6, 185e6, 175e6, 169e6,
159e6, 145e6, 132e6, 118e6, 102e6, 82e6, 69e6];
ym_grc =
[112000e6,112000e6,110348e6,108696e6,107044e6,105392e6,103740e6,102088e6,1004
36e6,98784e6,97132e6,95480e6,93828e6,92176e6,90525e6,88873e6];
E = interp1(temp_grc,ym_grc,temp,'linear','extrap');
YS = interp1(temp_grc,ys_grc,temp,'linear','extrap');

elseif material == 2
temp_inc = [273,473,673,773,873,1073];
ys_inc = [1206e6,1123e6,1075e6,1069e6,1025e6,755e6];
ym_inc = [250000e6,245000e6,240000e6,235000e6,230000e6,220000e6];
E = interp1(temp_inc,ym_inc,temp,'linear','extrap');
YS = interp1(temp_inc,ys_inc,temp,'linear','extrap');

elseif material == 3
temp_nbc = [300,700,1100,1500,1900];
ys_nbc = [208e6, 190e6, 169e6, 118e6, 69e6];
ym_nbc = [105000e6,84000e6,78750e6,73500e6,52500e6];
E = interp1(temp_nbc,ym_nbc,temp,'linear','extrap');
YS = interp1(temp_nbc,ys_nbc,temp,'linear','extrap');

elseif material == 4
temp_wre =
[300,350,400,450,500,550,600,650,700,750,800,850,900,950,1000,1050,1100,1150,
1200,1250,1300,1350,1400,1450,1500,1550,1600,1650,1700,1750,1800,1850,1900];
ys_wre =
[973e6,951.9e6,930.9e6,909.9e6,888.8e6,867.8e6,846.8e6,825.7e6,804.7e6,783.7e
6,762.6e6,741.6e6,720.6e6,699.5e6,678.5e6,657.5e6,636.5e6,615.4e6,594.4e6,573
.4e6,552.3e6,531.3e6,510.3e6,489.2e6,468.2e6,447.2e6,426.1e6,405.1e6,384.1e6,
363.0e6,342.0e6,321.0e6,300e6];
ym_wre =
[430000e6,407874.4e6,405528.9e6,403183.4e6,400837.8e6,398492.3e6,396146.8e6,3
93801.3e6,391455.7e6,389110.2e6,386764.7e6,384419.2e6,382073.6e6,379728.1e6,3
77382.6e6,375037.1e6,372691.5e6,370346.0e6,368000.5e6,365655.0e6,363309.4e6,3
60963.9e6,358618.4e6,356272.9e6,353927.3e6,351581.8e6,349236.3e6,346890.8e6,3
44545.2e6,342199.7e6,339854.2e6,337508.7e6,335163.1e6];
E = interp1(temp_wre,ym_wre,temp,'linear','extrap');
YS = interp1(temp_wre,ys_wre,temp,'linear','extrap');

end

end

```

function “calcDynamic” called within the “wall_temp_sweeps_R6_fn” function:

```

function [dynamicstress, vr] = calcDynamic(vs, E, tt, H, len, A_rat, rho, Pl,
Vcj)

% Calculates RDRE Combustor wall Response (Deflection, Bending moment Stress
& shear stress
% using an infinite beam on an elastic foundation model
%
%
%

```

```

%           Material Degradation and Design Considerations for
%           Regeneratively Cooled Rotating Detonation Rocket Engines, Davide
Vaccaro
%           Masters Thesis, Imperial College London/ Massachusetts Institute of
Technology
%           Supervisor: Prof. Zachary C Cordero

T=tt;

Ksystem=(E*len)/(H*(1-vs^2));% spring constant Pa
Kfoundation=Ksystem*len;% converts effective foundation modulus to a
foundation spring stiffness per unit length N/m

K = A_rat*Ksystem;

mass=rho*len*T;% mass per unit length 1 inch width by 1 inch
thickness(density * width)

I=(len*(T^3))/(12); %Second moment of area

EI=E*I ;
Z=T/2;% Distance from neutral axis, can vary this to find stress at
different points in the thickness

a=mass/(2*EI);
b=(K/EI)^0.5 ;
lam=(b/2)^0.5;% Lambda, normalised distance by this factor it is the
coefficient defining the static wave length, unit 1/m

P=P1* 1/lam ; % normalising Loading pressure

Vcr=((b)/a)^0.5 ; % Critical velocity of the system
vr=Vcj/Vcr;% velocity as a ratio of critical velocity
v=vr*Vcr;% velocity input
v2=vr^2;

x=linspace(0,1,10000); % discretiszing distance, in front of load,
circumferential distance
y=linspace(-1,0,10000); % distance behind the load, circumferential distance

% Static case
ws1=(exp(-lam.*x)).*(sin(x.*lam) + cos(lam.*x)); % Static deflection x > 0
ahead of wave
ws2=(exp(-lam.*x)).*(sin(x.*lam) + cos(lam.*y)); % Static deflection x<0
behind wave

bs1=(exp(-lam.*x)).*(-sin(x.*lam) + cos(lam.*x)); %Static bending moment x >
0
bs2=(exp(-lam.*y)).*(-sin(y.*lam) + cos(lam.*y)); %Static bending moment x<0

```

```

W0=(P*lam)/(2*K); % static deflection of beam
W0B=P/(4*lam);    % static BM of beam
%W0S=P; % static shear stress of beam

stress0=W0B*(Z/I) ; % calculating stress on the combustor wall directly under
load

W1s=W0*ws1; % deflection distribution
W2s=W0*ws2;

dist_vec=[y,x];
time_vec=dist_vec/Vcj;

staticdeflection=[ws1,ws2]; %changed this to include ws2

staticbm=[bs1,bs2]; %changed this to include bs2

if vr > 1 %Supercritical

A1=(v2+1)^0.5 + (v2 -1)^0.5 ; % A1 A2 REVERESED ONLY FOR THIS SCRIPT
A2=(v2+1)^0.5 - (v2 -1)^0.5 ;
A3=((v2^2)-1)^0.5 ;

%Deflection
W1=(( -2)/(A3*A1))*(sin(A1*(x*lam))) ;% for x>0 Deflection
W2=(( -2)/(A3*A2))*(sin(A2*(y*lam))) ;% for x<0

%Bending moment
W1B=(( -A1)/(A3)).*(sin(lam.*A1.*x)) ;% for x>0
W2B=(( -A2)/(A3)).*(sin(lam.*A2.*y)) ;% for x<0

dynamicbml=[W2B,W1B];
d_stress_vec=-W0B*dynamicbml*(Z/I) ;
deflec_dist=[W2s,W1s];

W1M=max(W1B); W2M=max(W2B); W1sM=max(W1s); W2sM=max(W2s);

%STRESSSS
stress1=-W0B*W1M*(Z/I) ;
stress2=-W0B*W2M*(Z/I) ;

mstr=max(stress1, stress2);
dynamicstress=mstr;

end

if vr < 1 % subcritical

ap=(1+v2)^0.5;
bp=(1-v2)^0.5 ;

%Deflection

```

```

W1s=((exp(-bp.*(x.*lam))).*(ap.*cos(ap.*(x.*lam)) +
bp.*sin(ap.*(x.*lam))))./(ap.*bp) ;% for x>0
W2s=((exp(-bp.*(-(y.*lam))).*(ap.*cos(ap.*(y.*lam)) + bp.*sin(ap.*(-
(y.*lam))))./(ap.*bp) ; % for x<0

%Bending moment calc
W1BB=((exp(-bp.*(x.*lam))).*(ap.*cos(ap.*(x.*lam)) -
bp.*sin(ap.*(x.*lam))))./(ap.*bp) ;% for x>0
W2BB=((exp(-bp.*(-(y.*lam))).*(ap.*cos(ap.*(y.*lam)) - bp.*sin(ap.*(-
(y.*lam))))./(ap.*bp) ; % for x<0

dynamicbml=[W2BB,W1BB];
d_stress_vec=-W0B*dynamicbml*(Z/I) ;
deflec_dist=[W2s,W1s];

W1M=max(W1BB); W2M=max(W2BB); % Max values

%STRESSSS
stress1=-W0B*W1M*(Z/I) ;
stress2=-W0B*W2M*(Z/I) ;

mstr=max(stress1, stress2);
dynamicstress=mstr;
end

end

```

function “config_check_R2_fn” called in the main run script:

```

function [metal_temp, fuel_temp, channel_delp, Re] =
config_check_R2_fn(material, h, b, t, s, mdot_f)

% Eric Jorgensen, MIT 2021, Master's thesis RDRE combustor optimization

% sets the material properties based on the flag passed for material
if material == 1
    k = 304;
elseif material == 2
    k = 11.4;
elseif material == 3
    k = 37.4;
elseif material == 4
    k = 70;
end

% reference mdot_f and heat flux to use in bartz equation scaling. this
% ties the input fuel flow rate to the heat flux in the temperature
% calculations
mdot_ref = 0.5; % kg/s
q_ref = 10e6; % W/m^2

% coolant properties for RP-1, density and inlet/outlet temps of ~300 and
% 600K, average viscosity over that range, average thermal conductivity
% over that range. inlet coolant temp, average specific heat over

```

```

% temperature range
rho_c_1 = 805;
rho_c_2 = 587;
mu = 5.64684E-05;
k_c = 0.077918;
Tc_in = 293+0;
Cp_1 = 2651;
Pran = Cp_1*mu/k_c;

% combustor axial length
L_comb=0.0254*1.5;

% calculate q value based on Bartz scaling relationship
q = q_ref * (2*(mdot_f/2)/mdot_ref)^(0.8);

% based on the channel spacing and channel support width, the number of
% discrete channels is calculated and channel characteristic dimensions
% such as hydraulic diameter
A_sect=h*L_comb;
n_cell=L_comb/(b+s);
A_rat=(b*n_cell)/((b+s)*n_cell);
A_flow_c = A_sect*(1-A_rat);
channel_arc_OD = L_comb*(1-A_rat)/n_cell;
channel_arc_ID = channel_arc_OD;
cooling_channel_area = A_flow_c/n_cell;
cooling_channel_perim = channel_arc_OD+channel_arc_ID+2*h;
d_h = 4*cooling_channel_area/cooling_channel_perim;

% for the outer body, the length of the channel is based on the
% flowpath/hotwall diameter plus the thickness of the hot wall.
L_channel=2*pi*((.0381+t));

% flow velocity is calculated based on m_dot = rho*V*A relationship. area
% is established above, derived from channel height, channel width, and
% channel support width. mdot_f is divided by 2 here since half the fuel
% flow would be used to cool the outer body and half would be used for the
% center body
v_c = (mdot_f/2)/((rho_c_1+rho_c_2)*A_flow_c);

% Reynolds number, friction factor, and convective heat transfer coefficient
% is calculated based on turbulent flow through pipe equations/correlations
Re_d = ((rho_c_1+rho_c_2)/2*v_c*d_h)/mu;
fric = 0.0791*(Re_d)^(-1/4);
h_c = k_c/d_h*((fric/2)*(Re_d-1000)*Pran)/(1+12.7*sqrt(fric/2)*(Pran^(2/3)-1));

% thermal resistance values calculated based on equations from Valdevit "A
% materials selection protocol for lightweight actively cooled panels"
r_1 = 1/2*(t/k);
r_2w = 1/2*(t/k)+1/h_c;
r_h = ((channel_arc_ID+b/2)/2)/k;
r_2c = 1/2*(t/k)+(atanh(sqrt((2*h_c)/(k*b)*h^2)))*(sqrt(2*h_c/(k*b))*k)^(-1);

% fuel temperature equation

```

```

T_fuel =
(q*L_channel)/((rho_c_1+rho_c_2)/2*Cp_1*v_c*(b+channel_arc_ID))+Tc_in;

% setting up systems of equation for linear system solve, added fixed
% heatflux BC, otherwise same as Valdevit system
A = [-1 0 0 (2*t*r_2w/channel_arc_ID) 0 (r_1+r_2w); -1 0 0 (-2*t*r_2c/b)
(r_1+r_2c) 0; 1 -1 0 0 0 -r_1; 1 0 -1 0 -r_1 0; 0 -1 1 -r_h 0 0; 0 0 0 0 b
channel_arc_ID];
b_rhs = [-T_fuel; -T_fuel; 0; 0; 0; q*(b+channel_arc_ID)];

x = linsolve(A,b_rhs);

T_m_channel_out = x(1);

% pressure drop calculated based on coolant flow characteristics
del_P = ((.3164*((rho_c_1+rho_c_2)/2*v_c*d_h/mu)^(-
1/4))/4*L_channel/d_h*((rho_c_1+rho_c_2)/2*v_c*A_flow_c)/A_flow_c)^2*(1/rho_
c_1+1/rho_c_2))/10^6;

% re-assigning variable names to output from function
metal_temp=T_m_channel_out;
fuel_temp=T_fuel;
channel_delP=del_P;
Re=Re_d;

% filter out design configurations where r_2c value becomes imaginary. r_2c
% varies (approximately) linearly with fuel flow rate. this relationship
% was calculated using linear regression and used to smooth out noise
% caused by imaginary number for the output plots
real_check = isreal(r_2c);
if (real_check == 0)
    metal_temp=0;
    fuel_temp=0;
    channel_delP=0;
    Re=0;
end
end

```

Bibliography

- [1] Boller, S. A. *Flow Behavior in Radial Rotating Detonation Engines*. Air Force Institute of Technology, 2019.
- [2] Khan, T., and Qamar, I. “Factors Affecting Characteristic Length of the Combustion Chamber of Liquid Propellant Rocket Engines.” *Mehran University Research Journal of Engineering and Technology*, Vol. 38, No. 3, 2019, pp. 729–744. <https://doi.org/10.22581/muet1982.1903.16>.
- [3] Braun, E. M., Lu, F. K., Wilson, D. R., and Camberos, J. A. “Airbreathing Rotating Detonation Wave Engine Cycle Analysis.” *Aerospace Science and Technology*, Vol. 27, No. 1, 2013, pp. 201–208. <https://doi.org/10.1016/j.ast.2012.08.010>.
- [4] Hargus, W. A., Schumaker, S. A., and Paulson, E. J. “Air Force Research Laboratory Rotating Detonation Rocket Engine Development.” *AIAA Propulsion and Energy*, 2018. <https://doi.org/10.2514/6.2018-4876>.
- [5] J. Shaw, I., A.C. Kildare, J., J. Evans, M., Chinnici, A., A.M. Sparks, C., N.H. Rubaiyat, S., C. Chin, R., and R. Medwell, P. A Theoretical Review of Rotating Detonation Engines. In *Direct Numerical Simulations - An Introduction and Applications* (S. Rao, ed.), IntechOpen, 2021.
- [6] Zhou, R., Wu, D., and Wang, J. “Progress of Continuously Rotating Detonation Engines.” *Chinese Journal of Aeronautics*, Vol. 29, No. 1, 2016, pp. 15–29. <https://doi.org/10.1016/j.cja.2015.12.006>.
- [7] Coleman, M. L. *Overview of Pulse Detonation Propulsion Technology*. Publication CPTR 70. Chemical Propulsion Information Agency, 2001, p. 64.
- [8] Lu, F. K., and Braun, E. M. “Rotating Detonation Wave Propulsion: Experimental Challenges, Modeling, and Engine Concepts.” *Journal of Propulsion and Power*, Vol. 30, No. 5, 2014, pp. 1125–1142. <https://doi.org/10.2514/1.B34802>.
- [9] Wang, Z., Wang, Y., Peng, C., and Zheng, L. “Experimental Study of Pressure Back-Propagation in a Valveless Air-Breathing Pulse Detonation Engine.” *Applied Thermal Engineering*, Vol. 110, 2017, pp. 62–69. <https://doi.org/10.1016/j.applthermaleng.2016.08.144>.
- [10] Wolański, P. “Detonative Propulsion.” *Proceedings of the Combustion Institute*, Vol. 34, No. 1, 2013, pp. 125–158. <https://doi.org/10.1016/j.proci.2012.10.005>.
- [11] Li, J.-M., Teo, C. J., Khoo, B. C., Wang, J.-P., and Wang, C., Eds. Review on the Research Progresses in Rotating Detonation Engine. In *Detonation Control for Propulsion*, Springer International Publishing, Cham, 2018, pp. 109–154.

- [12] Bykovskii, F. A., Zhdan, S. A., and Vedernikov, E. F. “Continuous Spin Detonations.” *Journal of Propulsion and Power*, Vol. 22, No. 6, 2006, pp. 1204–1216. <https://doi.org/10.2514/1.17656>.
- [13] Sosa, J., Burke, R., Ahmed, K. A., Micka, D. J., Bennewitz, J. W., Danczyk, S. A., Paulson, E. J., and Hargus, W. A. “Experimental Evidence of H₂/O₂ Propellants Powered Rotating Detonation Waves.” *Combustion and Flame*, Vol. 214, 2020, pp. 136–138. <https://doi.org/10.1016/j.combustflame.2019.12.031>.
- [14] Ishihara, K., Nishimura, J., Goto, K., Nakagami, S., Matsuoka, K., Kasahara, J., Matsuo, A., Funaki, I., Moriai, H., Mukae, H., Yasuda, K., Nakata, D., and Higashino, K. “Study on a Long-Time Operation Towards Rotating Detonation Rocket Engine Flight Demonstration.” *AIAA SciTech*, 2017. <https://doi.org/10.2514/6.2017-1062>.
- [15] Micka, D. J., Daines, G., Sosa, J., Burke, R. F., Ahmed, K. A., Paulson, E., Bennewitz, J. W., Danczyk, S., and Hargus, W. A. “Heat Transfer Measurements in an Elevated Pressure RDRE Combustor.” *AIAA Propulsion and Energy*, 2021. <https://doi.org/10.2514/6.2021-3685>.
- [16] Theuerkauf, S. W., Schauer, F., Anthony, R., and Hoke, J. Experimental Characterization of High-Frequency Heat Flux in a Rotating Detonation Engine. Presented at the 53rd AIAA Aerospace Sciences Meeting, Kissimmee, Florida, 2015.
- [17] Pizzarelli, M. “Dataset of the Experimentally Measured Heat Transfer in the Throat Region of Liquid Rocket Engine Thrust Chambers.” *Data in Brief*, Vol. 37, 2021, p. 107173. <https://doi.org/10.1016/j.dib.2021.107173>.
- [18] Li, J.-M., Teo, C. J., Khoo, B. C., Wang, J.-P., and Wang, C., Eds. Application of Detonation Waves to Rocket Engine Chamber. In *Detonation Control for Propulsion*, Springer International Publishing, Cham, 2018, pp. 109–154.
- [19] Goto, K., Nishimura, J., Kawasaki, A., Matsuoka, K., Kasahara, J., Matsuo, A., Funaki, I., Nakata, D., Uchiumi, M., and Higashino, K. “Propulsive Performance and Heating Environment of Rotating Detonation Engine with Various Nozzles.” *Journal of Propulsion and Power*, Vol. 35, No. 1, 2019, pp. 213–223. <https://doi.org/10.2514/1.B37196>.
- [20] Theuerkauf, S., King, P., Schauer, F., and Hoke, J. “Thermal Management for a Modular Rotating Detonation Engine.” *51st AIAA Aerospace Sciences Meeting*, 2013. <https://doi.org/10.2514/6.2013-1176>.
- [21] Vermaak, N., Valdevit, L., and Evans, A. G. “Materials Property Profiles for Actively Cooled Panels: An Illustration for Scramjet Applications.” *Metallurgical and Materials Transactions A*, Vol. 40, No. 4, 2009, pp. 877–890. <https://doi.org/10.1007/s11661-008-9768-y>.
- [22] Vermaak, N., Valdevit, L., and Evans, A. G. “Influence of Configuration on Materials Selection for Actively Cooled Combustors.” *Journal of Propulsion and Power*, Vol. 26, No. 2, 2010, pp. 295–302. <https://doi.org/10.2514/1.45417>.

- [23] Valdevit, L., Vermaak, N., Zok, F. W., and Evans, A. G. “A Materials Selection Protocol for Lightweight Actively Cooled Panels.” *Journal of Applied Mechanics*, Vol. 75, No. 6, 2008, p. 061022. <https://doi.org/10.1115/1.2966270>.
- [24] Valdevit, L., Vermaak, N., Hsu, K., Zok, F., and Evans, A. “Design of Actively Cooled Panels for Scramjets.” *AIAA/AHI Space Planes and Hypersonic Systems and Technologies*, 2006. <https://doi.org/10.2514/6.2006-8069>.
- [25] Tang, S.-C. “Dynamic Response of a Tube Under Moving Pressure.” *Journal of the Engineering Mechanics Division*, Vol. 91, No. 5, pp. 97–122.
- [26] Beltman, W. M., and Shepherd, J. E. “Linear Elastic Response of Tubes to Internal Detonation Loading.” *Journal of Sound and Vibration*, Vol. 252, No. 4, 2002, pp. 617–655. <https://doi.org/10.1006/jsvi.2001.4039>.
- [27] Austral Wright Metals. Copper Alloys C11000 ETP. <https://www.australwright.com.au/technical-data/alloys/copper-brass/c11000-etp-copper/>. Accessed Nov. 2, 2021.
- [28] Minneci, R. P., Lass, E. A., Bunn, J. R., Choo, H., and Rawn, C. J. “Copper-Based Alloys for Structural High-Heat-Flux Applications: A Review of Development, Properties, and Performance of Cu-Rich Cu–Cr–Nb Alloys.” *International Materials Reviews*, Vol. 66, No. 6, 2021, pp. 394–425. <https://doi.org/10.1080/09506608.2020.1821485>.
- [29] Maher. Alloy 718 Data Sheet. <https://www.maher.com/media/pdfs/718-datasheet.pdf>. Accessed Jun. 29, 2021.
- [30] Carpenter. Pyromet Alloy 718 Datasheet. <https://www.spacematdb.com/spacemat/manudatasheets/inconel%20718.pdf>.
- [31] Antoine, C., Foley, M., and Dhanaraj, N. *Physical Properties of Niobium and Specifications for Fabrication of Superconducting Cavities*. Publication FERMILAB-TM-2503-TD, 1022786. 2006.
- [32] Wojcik, C. C. *Thermomechanical Processing and Properties of Niobium Alloys*. Wah Chang, An Allegheny Technologies Company.
- [33] Jun, C. K., and Hoch, M. *Thermal Conductivity of Tantalum, Tungsten, Rhenium, Ta-10W, T111, T222, W-25Re, in the Temperature Range 1500-2800 K*. Publication AFML-TR-66-367. Air Force Materials Laboratory, 1966.
- [34] Rhenium. Mechanical and Physical Properties. http://rhenium.com/assets/tungsten-rhenium_alloys_properties.pdf. Accessed Apr. 10, 2021.
- [35] Khoele, K., and Delport, D. J. “Mechanical and Corrosion Behavior of Inconel 718 Nickel-Based Super Alloy Doped with Graphene Nanoplatelets.” *Journal of Failure Analysis and Prevention*, Vol. 19, No. 5, 2019, pp. 1493–1497. <https://doi.org/10.1007/s11668-019-00754-3>.

- [36] Extreme Bolt & Fastener. Technical Data Inconel 718. <https://www.extreme-bolt.com/inconel-718-fasteners-flanges.html>. Accessed Jun. 29, 2021.
- [37] Prasad, N. E., and Wanhill, R. J. H., Eds. Niobium and Other High Temperature Refractory Metals for Aerospace Applications. In *Aerospace Materials and Material Technologies*, Springer Singapore, Singapore, 2017, p. 269.
- [38] Leonhardt, T. “Properties of Tungsten-Rhenium and Tungsten-Rhenium with Hafnium Carbide.” *JOM*, Vol. 61, No. 7, 2009, pp. 68–71. <https://doi.org/10.1007/s11837-009-0107-6>.
- [39] Frost, H., and Ashby, M. The f.c.c. Metals: Ni, Cu, Ag, Al, Pb and γ -Fe. In *Deformation-Mechanism Maps, The Plasticity and Creep of Metals and Ceramics*.
- [40] Titran, R. H., and Klopp, W. D. *Long-Time Creep Behavior of the Niobium Alloy C-103*. Publication NASA Technical Paper 1727. 1980.
- [41] Bennewitz, J. W., Burr, J. R., and Lietz, C. F. “Characteristic Timescales for Rotating Detonation Rocket Engines.” *AIAA Propulsion and Energy*, 2021. <https://doi.org/10.2514/6.2021-3671>.
- [42] Magee, J. W., Bruno, T. J., Friend, D. G., Huber, M. L., Laesecke, A., Lemmon, E. W., McLinden, M. O., Perkins, R. A., Baranski, J., and Widegren, J. A. *Thermophysical Properties Measurements and Models for Rocket Propellant RP-1: Phase I*. Publication NISTIR 66476. National Institute of Standards and Technology, 2007.
- [43] Outcalt, S. L., Laesecke, A., and Brumback, K. J. “Thermophysical Properties Measurements of Rocket Propellants RP-1 and RP-2.” *Journal of Propulsion and Power*, Vol. 25, No. 5, 2009, pp. 1032–1040. <https://doi.org/10.2514/1.40543>.
- [44] Abdulagatov, I. M., and Azizov, N. D. “Heat Capacity of Rocket Propellant (RP-1 Fuel) at High Temperatures and High Pressures.” *Fuel*, Vol. 90, No. 2, 2011, pp. 563–567. <https://doi.org/10.1016/j.fuel.2010.09.038>.
- [45] Vlasov, V. Z., and Leont’ev, N. N. Plane Model of the Elastic Foundation with Two Characteristics. In *Beams, Plates and Shells on Elastic Foundations*, pp. 13–16.
- [46] Kenney Jr., J. T. “Steady State Vibrations of Beam on Elastic Foundation for Moving Load.” *Journal of Applied Mechanics*.
- [47] Kanda, T., Sato, M., Kimura, T., and Asakawa, H. “Expander and Coolant-Bleed Cycles of Methane-Fueled Rocket Engines.” *Transactions of the Japan Society for Aeronautical and Space Sciences*, Vol. 61, No. 3, 2018, pp. 106–118. <https://doi.org/10.2322/tjsass.61.106>.